THESIS APPROVAL

GRADUATE SCHOOL, KASETSART UNIVERSITY

Master of Science (Physics)
DEGREE

Physics
FIELD

Physics
DEPARTMENT

TITLE: Development of Flexible Gas Sensors Based on Ink-jet Printing Method

NAME: Mr. Yotsarayuth Seekaew

THIS THESIS HAS BEEN ACCEPTED BY

THESIS ADVISOR
(Mr. Chatchawal Wongchoosuk, Ph.D.)

DEPARTMENT HEAD
(Assistant Professor Surasak Chiangga, Dr.rer.nat.)

APPROVED BY THE GRADUATE SCHOOL ON

DEAN
(Associate Professor Gunjana Theeragool, D.Agr.)

THESIS

DEVELOPMENT OF FLEXIBLE GAS SENSORS BASED ON INK-JET PRINTING METHOD

YOTSARAYUTH SEEKAEW

A Thesis Submitted in Partial Fulfillment of
the Requirements the Degree of
Master of Science (Physics)
Graduate School, Kasetsart University
2014

Yotsarayuth Seekaew 2014: Development of Flexible Gas Sensors Based on Ink-jet Printing Method. Master of Science (Physics), Major Field: Physics, Department of Physics. Thesis Advisor: Mr. Chatchawal Wongchoosuk, Ph.D. 60 pages.

This work presents a simple, low-cost and practical inkjet-printing technique for fabricating innovative flexible gas sensors made of Poly(3,4-ethylenedioxythiophene): Polystyrene sulfonate (PEDOT:PSS) conducting polymer and graphene material composite film with high uniformity over a large area. The fabricated flexible gas sensors have been investigated for ammonia (NH_3) detection at room temperature. Transmission electron microscopy (TEM), Atomic force microscopy (AFM), Fourier transform infrared spectroscopy (FTIR), UV-visible spectrometer and Raman spectroscopy were used to characterize the morphology and formation mechanism of printed sensing films. The results show that the electrical resistance of the films decreases with increasing film thickness. The based line resistance of sensing film can change on time due to humidity effect. The heating temperature of 90 ^{0}c for 20 min can correct the drift effect and recover the based line resistance to the original sensor. AFM results show an increase of surface roughness after adding of graphene into PEDOT:PSS. It suggests a significant enhancement of the active surface-area for gas adsorption by graphene. TEM, FTIR and Raman characterizations confirm the presence of few-layer graphene in PEDOT:PSS polymer matrix and the present of $\pi - \pi$ interactions between graphene and PEDOT: PSS. The ink-jet printed graphene-PEDOT:PSS gas sensor exhibits high response and high selectivity to NH_3 in a low concentration range of 25-1000 ppm at room temperature. The sensing mechanism of graphene-PEDOT:PSS sensor has been discussed in term of three possible mechanisms; (I) reducing reaction, (II) direct charge transfer process, and (III) swelling process.

Student's signature   Thesis Advisor's signature   ___ / ___ / ___

ACKNOWLEDGEMENTS

For the success of my thesis, I would like to give special thank to Dr. Chatchawal Wongchoosuk, my thesis for advisor, encouragement and valuable suggestion for completely writing of thesis. I would sincerely like to thank Asst. Prof. Dr. Teerakiat Kerdcharoen and Mr. Shongpun Lokavee for valuable suggestion and kindly providing materials (PEDOT:PSS, graphene powder) for using in this research. I am heartfelt thank to my friends from Center of Nanoscience and Nanotechnology ,Faculty of Science, Mahidol University, Thailand and Laboratory for Multiscale Innovative Technologies (LMIT), Department of Physics, Faculty of Science, Kasetsart University, Thailand.

I gratefully thank Dr. Anurat Wisitsoraat and Mr. Ditsayut Phokharatkul from Nanoelectronics and MEMS Laboratory, National Electronics and Computer Technology Center, Thailand, for equipment supports (AFM, Raman, SEM, TEM) for result analysis.

This research was supported by the Graduate School, Kasetsart University and the Kasetsart University Research and Development Institute (KURDI) for financial support of this thesis.

Finally, I most gratefully acknowledge my parents and my friends for all their supports throughout the period of this research.

Yotsarayuth Seekaew
June 2014

TABLE OF CONTENTS

Page

LIST OF TABLES

Table **Page**

LIST OF FIGURES

Figure **Page**

LIST OF FIGURES (Continued)

LIST OF FIGURES (Continued)

Figure **Page**

LIST OF ABBREVIATIONS

PEDOT:PSS = Poly(3,4-ethylenedioxythiophen/poly(styrenesulfonate)
NH_3 = Ammonia
ppm = part per million
g = gram
ml = microliter
GO = Graphene oxide
DMSO = Dimethyl sulfoxide
EG = Ethylene glycol
TEM = transmission electron microscopy
AFM = Atomic force microscopy
SEM = Scanning electron microscope
FTIR = Fourier transform infrared spectroscopy
nm = nanometer
cm = centimeter
mg = milligram
µm = micrometer
V = voltage
VOCs = volatile organic compounds
R = Resistance
C = carbon
H = hydrogen
O = oxygen
N = nitrogen
S = sulfur
°C = degree Celsius

DEVELOPMENT OF FLEXIBLE GAS SENSORS BASED ON INK-JET PRINTING METHOD

INTRODUCTION

Nowadays, gas sensor can be fabricated by several techniques such as thermal evaporation, Langmuir-Blodgett technique, spin coating, drop-coating, reactive sputtering, and screen printing. Although these techniques have been successfully used in fabrication of gas sensors, many of them do not support the preparation of film on flexible substrates such as paper or plastic. Moreover, some of the techniques have disadvantages such as high cost, complicated, long-time operations, low reliability and low-productivity. Very recently, a promising method for gas sensor preparation was proposed by using ink-jet printing technique because of its many unique advantages such as low temperature processing, high productivity, simplicity, low-cost, and low materials waste. It can control deposition of functional materials with arbitrary geometry on various types of substrate. The ink-jet printing has become a potential solution in material and device preparation.

Ammonia (NH_3) is a highly toxic and polluting gas. It is widely existed in the environment such as in air, soil, and water. Furthermore, ammonia has a wide variety of uses including the production of nitrogenous fertilizers and other nitrogenous chemicals, as well as an industrial refrigerant. Monitoring of leakage in a wide range of industrial applications is thus deeply desired. For humans, the skin, eyes and respiratory tract would be injured in the high concentration of NH_3. Also, NH_3 is flammable at the high concentration.

So far, a lot of researches have reported on developments of NH_3 sensor based on metal oxide semiconductors which may be expensive, operated at high temperature, high power consumption and low sensitivity. Therefore, fabrication of the NH_3 gas sensor with reliable, low-cost, high productivity, simplicity, low materials waste and operation at room temperature is urgent and significant for human demand. In this work, the flexible gas sensors have been developed by using ink-jet printing method. The development of a flexible gas sensor was used to detect toxic gas such as NH_3. Moreover, it will be useful for development of future wearable electronic technology.

OBJECTIVES

1. To fabricate the flexible low-cost gas sensors by ink jet printing technique.

2. To design the interdigitated electrodes of gas sensor using aluminium tape and conductive silver paint for good performance in response on target gas.

3. To study the properties and the morphologies of printed sensing films.

4. To study the response of the gas sensor to various volatile organic compounds such as ethanol, methanol, toluene, acetone and ammonia.

LITERATURE REVIEW

Crowley et al. (2008) fabricated an ammonia gas sensor using inkjet-printed polyaniline nanoparticles. The synthesis of the polyaniline nanoparticle based on 0.6 ml of freshly distilled aniline, 3.4 g dodecylbenzenesulfonic acid (DBSA,TCI), and 0.36 g ammonium persulfate (APS) were added to 40 mldeionised water and stirred for 2.5 huntil. A dark green viscous solution was formed. NanoPANI-modified interdigitated electrode arrays (nanoPANI-IDAs) were fabricated using screen printing and inkjet printing methods. The electrode patterns were designed using AutoCAD (Autodesk). Silver and carbon IDA patterns were prepared using screen printing. Screen printing was performed using a DEK model 247 and the IDA patterns were printed on 175µm polyethylene terephthalate substrate and cured at 150 °C for 30 min.

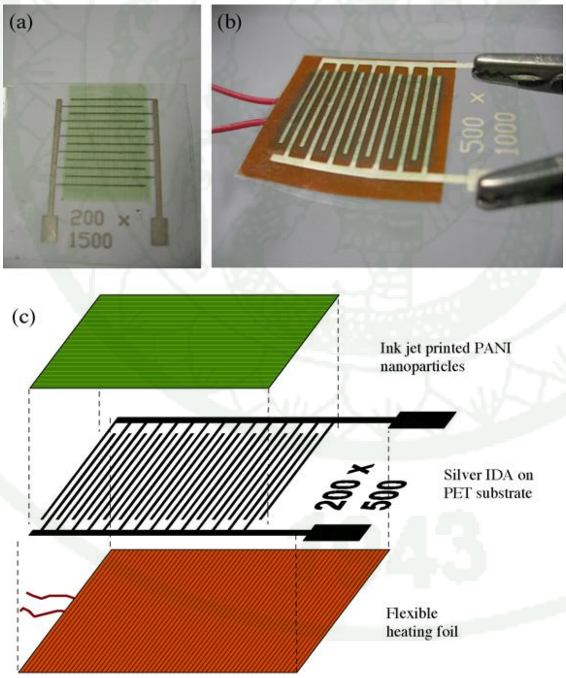

Figure 1 Polyaniline interdigitated electrodes (nanoPANI-IDAs) shown alone (a) and with a thermofoil heater (b). Exploded schematic diagram of the nanoPANI-IDA electrode showing the different layers of the sensor (c).

Source: Crowley *et al.*. (2008)

Inkjet printing was performed using unmodified Epson C46/C48 piezoelectric printers. Both the black and color printer cartridges were opened and the ink removed. The cartridges were rinsed thoroughly with deionised water prior to being refilled with the nanoPANI suspension. Print designs were drawn using standard Windows software (e.g. MS Word) and printing was performed through the supplied software in the standard way. The printer was first primed with standard cartridges and once good quality prints were obtained with the commercial ink. The cartridges were replaced with the nanoPANI cartridges. Priming the printer with the nanoPANI solution involved the use of cleaning cycles and ink purging features until a good quality print was achieved. Following printing, the sensors were gently rinsed in deionised water before being heat cured at 75 ◦C for 30 min. Sensors were also constructed by attaching polyimide-based flexible heating foils to the back of the PET substrate as shown in figure 1.

Loffredo et al. (2009) reported on the inkjet printing process aimed at producing sensor devices based on carbon black/polymer composite films. Ink was prepared by dissolving PS (80 mg) in hot NMP in a 0.5 wt% concentration. The filler (20 mg) was then dispersed in this polymeric solution by ultrasonic bath for 90 min. The final PS/CB suspension was filtered using a 0.2 µm Teflon filter to remove agglomerates larger than 0.2 µm. The fabrication process of the sensor devices consists of four steps. At the first, interdigitated metallic electrodes were realized on alumina substrate. The second step was the preparation of CB polymeric suspension. The third step was the sensing film deposition. Finally, the devices were mounted on a commercial TO8 case and characterized in the testing chamber. Three series of sensor devices were fabricated, the first was completely obtained using ink-jet technique either for the deposition of Ag contacts and for the sensing film deposition (series 1), the second was fabricated by ink-jetting the same sensing film (volume and geometry) on Au contacts made by a lift-off photolithographic process (series 2), the last series was prepared by casting deposition on the same Au contacts (series 3).
The quantitative responses obtained with sensors prepared by ink-jet processing (series 1 and 2) have been compared as shown in Fig. 2, with those of the series 3. All sensors series exhibit linear responses in the investigated range of concentrations. The series two sensors have higher response at 600ppm compared to other sensors while at 1200ppm and 2400ppm its response is similar to series 3 devices.

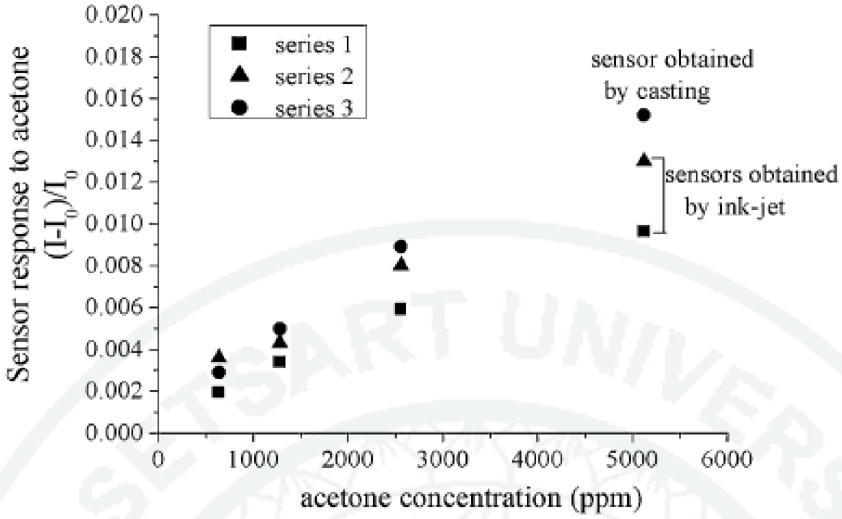

Figure 2 Responses at different concentrations of acetone for the sensor devices.

Source: Loffredo *et al*.. (2009)

Xu et al. (2009) have reported a novel hybrid material (graphene-PEDOT) with good organic solution-processability, excellent optical transparency, conductivity, and flexibility. The synthesis of the graphene-PEDOT hybrid was represented schematically in figure 3**.** The monomer 3,4-ethyldioxythiophene (EDOT) was polymerized *in situ* in a solution of sulfonated graphene to give graphene-PEDOT.

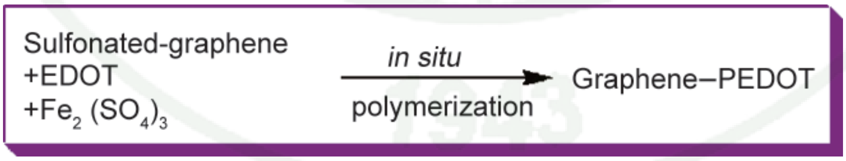

Figure 3 Scheme of synthesis of graphene-PEDOT. Reagents and conditions, Sulfonated graphene (10 mg), anhydrous $Fe_2(SO_4)_3$ (10 mg, 0.025 mmol), EDOT (100 mg, 0.70 mmol), H_2O (10 mL), 50 °C, 48 h.

Source: Xu *et al*.. (2009)

Huang et al. (2011) studied the inkjet printing to present using two types of graphene materials, namely single-layered graphene oxide (GO) and few-layered graphene oxide (FGO). Various high image quality patterns with controllable line-width and thickness were prepared on different commercial flexible substrates by the direct inkjet printing method using aqueous solutions of these two graphene materials. In the preparation of graphene inks, the printable graphene-based inks were prepared by sonicating 150 mg of GO or 120 mg of FGO in 15 mL of deionized water for 2 h. After sonication, the dispersed solutions were centrifuged at 6000 rpm for 15 min to remove large-sized particles of graphene material. Then, the residual suspension was filtered through a filter with 0.45-µm pore size. The poly(ethylene terephthalate) (PET) and polyimide (PI) were prepared for substrates of two graphene materials. Inkjet printing was carried out by using modified HP Deskjet K7108 printer at room temperature. The prepared ink was injected into a cleaned HP 853 ink cartridge by a syringe. Before printing, the ink cartridge was allowed to stand for several minutes to ensure the equilibration of the ink in the cartridge. Then, the patterns designed by Microsoft Powerpoint were printed onto the desired flexible substrates including normal printing paper, PET, and PI (see Fig. 4). In the preparation of electrochemical sensor, a graphene-based electrode was fabricated by using inkjet printing and annealing in Ar/H_2 and used as the working electrode, together with a Pt electrode and an Ag/AgCl electrode to form the electrochemical sensor system. Figure 3b shows that the conductivity of patterns printed using FGO ink is higher than that of printed GO ink for the same number of printing times.

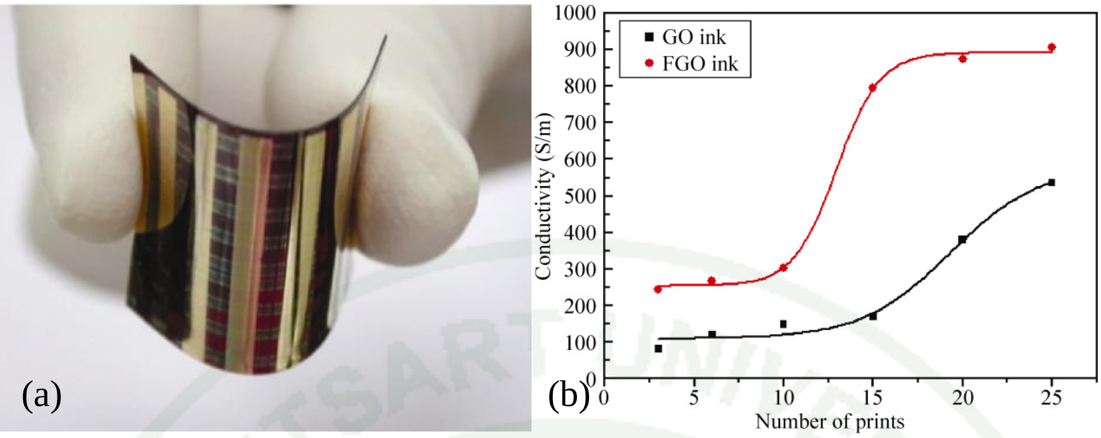

Figure 4 Photograph of a printed pattern on a PI substrate (a) and the relationship between the number of printing times and the electrical conductivity of the reduced patterns on PI (b).

Source: Huang *et al.*. (2011)

In 2012, Wongchoosuk *et al.* reported the fabrication of low-cost and flexible NH_3 gas sensor using inkjet printing technique on a basis of a novel sensor structure and electronic ink formula. In the preparation of electronic ink, the electronic ink was prepared based on the conjugated polymer poly(3,4-ethylene dioxythiophene) doped with polystyrene sulfonated acid (PEDOT/PSS) (BaytronP). A flexible gas sensor was fabricated by using modified Canon PIXMA iP4600 thermal printer with a resolution (BW) of 600 × 600 dpi. The electronic ink as a sensing film with rectangle geometry (1.5 cm x 2.5 cm) was directly printed on flexible substrate (photo paper). The simple interdigitated electrodes made from patterned aluminum plate with thickness of 35 µm were attached over the sensing film. From Fig. 5, it can be seen that PEDOT/PSS gas sensor exhibits a strong response to NH_3, and much weaker responses to ethanol, acetone, and toluene at room temperature. The sensor response works linearly with gas concentrations between 100-1000 ppm.

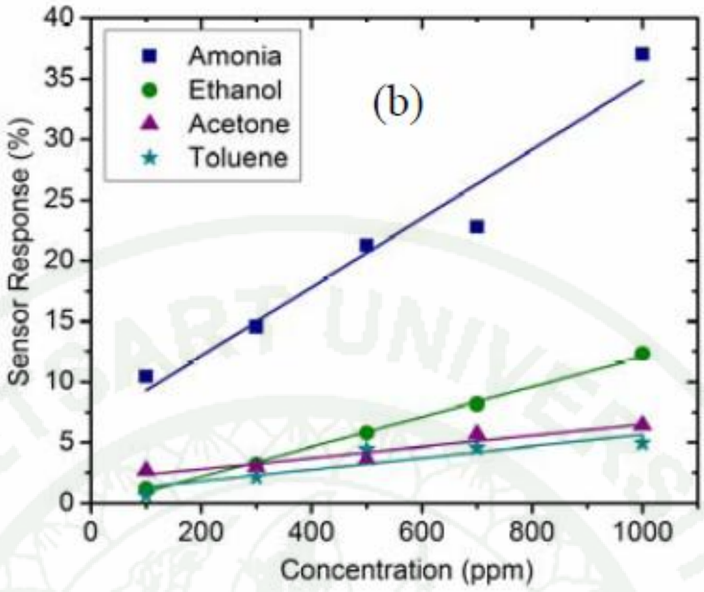

Figure 5 Sensing response of the gas sensor at room temperature.

Source: Wongchoosuk *et al.*. (2012)

Shen et al. (2012) have studied properties of SnO_2 based gas-sensing thin films prepared by ink-jet printing. The preparation of precursor inks and SnO_2 based thin films, both $SnCl_2 \cdot 2H_2O$ (0.05 mol) and oxalic acid (0.01 mol) were dissolved into 100 mL of anhydrous alcohol. This mixture was stirred for 1 h, resulting in a slightly turbid solution. This solution was marked as ink A and was used as the 0.5 mol/L SnO_2 precursor ink. 0.01 mol/L Au, Ag, Pd, Co, Ni, Cu, Sb or Zr was used for ink additives. This mixture then underwent ultrasonic dispersion for 15 min. The pure SnO_2 precursor ink and the different additive inks were loaded into different cartridges and then printed onto a monocrystalline silicon wafer or an alumina substrate coated with interdigital gold electrodes using modified ink jet printer. When printing was complete, the samples were kept in air at room temperature. After 24 h, the samples formed gelled films that were then sintered at 550 °C for 1 h.

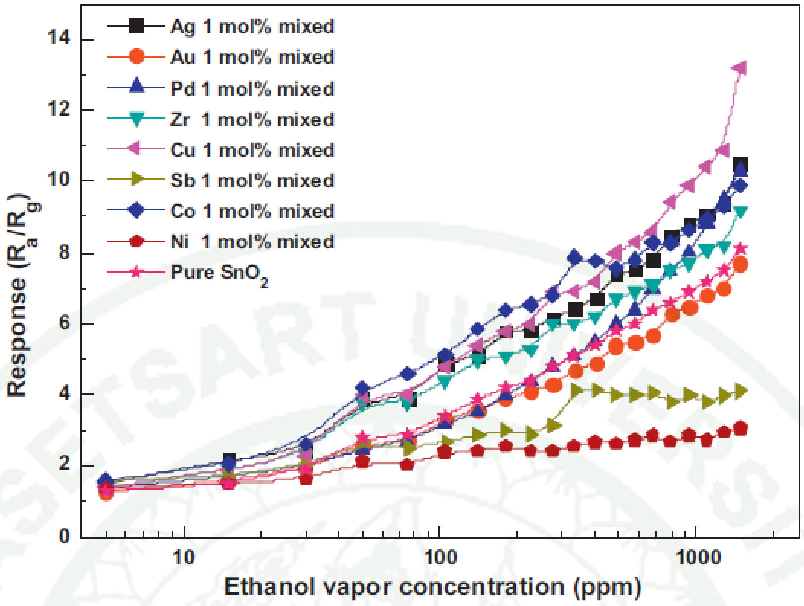

Figure 6 The response of SnO_2 based thin films printed four times to ethanol vapour at 350 °C.b

Source: Shen *et al*.. (2012)

The influence of additives on the response of SnO_2 films can be seen in Fig. 6. The response of a SnO_2 film formed by 4 printing events to ethanol vapour increased when the film was mixed with Ag, Co, Cu or Zr. The sample mixed with 1 mol% of Cu had the highest response when the concentration of ethanol vapour was over 500 ppm. The initial response of the pure SnO_2 film to 1475 ppm ethanol vapour was 8.1 at 350 °C. The response increased to 13.2 when the film was mixed with 1 mol% of Cu, and the response decreased to 3.1 when the film was mixed with 1 mol% Ni. The additive's effect on the films response to ethanol was significantly less when the film was mixed with 1 mol% Au or Pd and the ethanol concentration was below 500 ppm.

Lua et al. (2013) studies a new one-step electrochemical approach to the synthesis of high quality graphene-poly(3,4-ethylenedioxythiophene) (graphene–PEDOT) nanocomposite film on a glassy carbon (GC) electrode by using graphene oxide (GO) and PEDOT as the starting materials. The preparation of graphene composites, graphene film was electrochemically deposited on the GC electrode by cyclic voltammetry with potential scanning between -1.5 and 1.1 V with a sweep rate of 100 mV s^{-1} at room temperature for

10 cycles in a fresh solution containing 1.0 mg mL^{-1} GO and 0.01 M $LiClO_4$. PEDOT film was electrochemically deposited on the GC electrode by cyclic voltammetry with potential scanning between -0.9 and 1.1 V with a sweep rate of 100 mV s^{-1} at room temperature for 10 cycles in a fresh solution containing 0.01 M EDOT and 0.01 M $LiClO_4$. Graphene–PEDOT nanocomposite film was electrochemically deposited on the GC electrode by cyclic voltammetry with potential scanning between -1.5 and 1.1 V with a sweep rate of 100 mV s^{-1} at room temperature for 10 cycles in a fresh solution containing 1.0 mg mL^{-1} GO, 0.01 M EDOT monomer and 0.01 M $LiClO_4$. After deposition, these working electrodes were washed with distilled water (see in Figure 7).

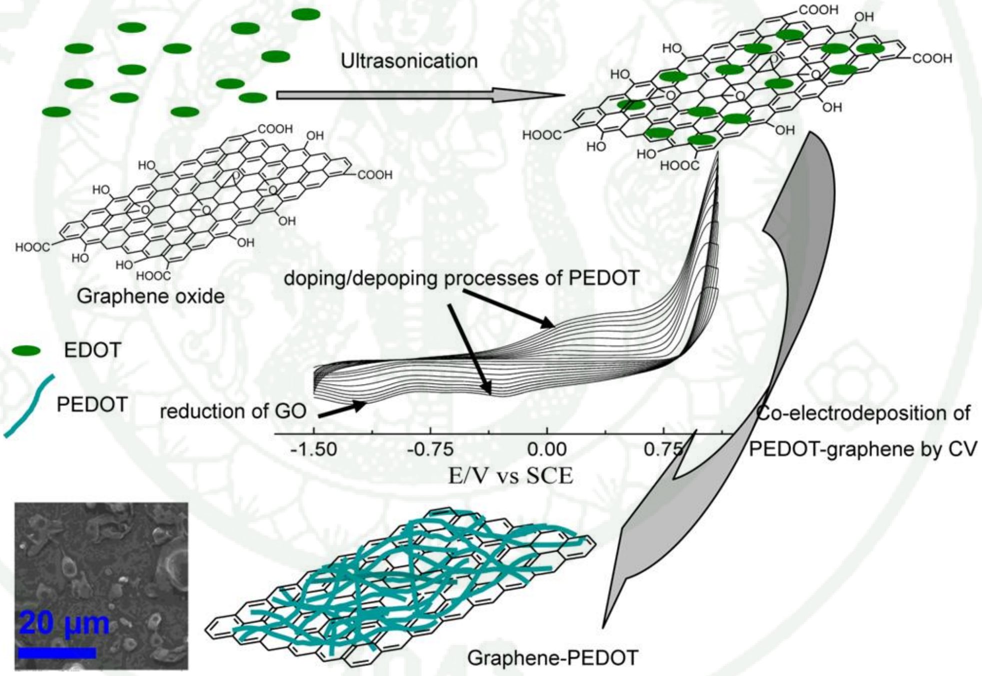

Figure 7 Schematic illustration for the synthesis of graphene–PEDOT by a facile one-step redox route.

Source: Lu *et al.*. (2013)

SEM was used to characterize the graphene-PEDOT nanocomposite. The SEM images of PEDOT film, graphene and graphene-PEDOT nanocomposite film are shown in Fig. 8A-C, respectively. The pure PEDOT film (Fig. 8A) presents a rather regular, smooth and homogeneous structure. Fig. 8B shows the SEM image of electrochemically synthesized graphene, displaying their well exfoliated, typical wrinkled surface morphology. The in situ electrochemically deposited grapheme-PEDOT nanocomposite film (Fig. 8C) manifests the mixed morphology of the wrinkled graphene covered by PEDOT obtained by the polymerization of EDOT monomer.

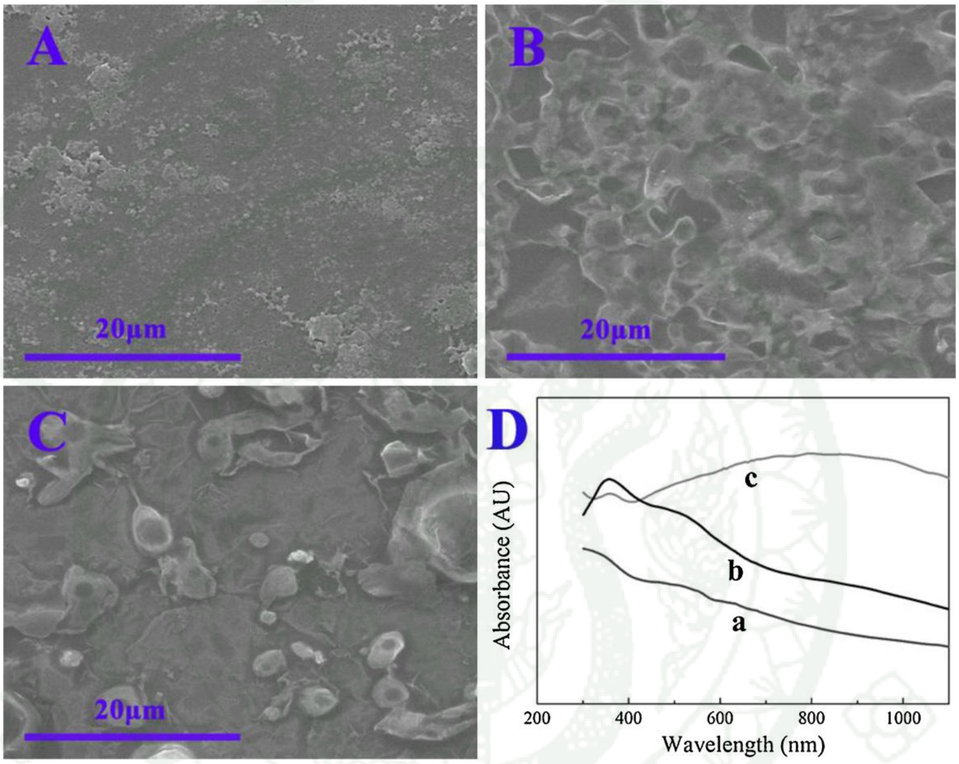

Figure 8 The SEM images of PEDOT film (A), graphene (B) and graphene–PEDOT nanocomposite film (C), UV–vis spectra of (a) graphene, (b) PEDOT, and (c) graphene/PEDOT composite film (D).

Source: Lua *et al.*. (2013)

Theory

1. Ink-jet printing

Ink-jet printing technique is becoming an attractive technology in preparation of thin film. Mohammed *et al*. (2006) explained that the method works by ejecting ink through very fine nozzles, 10–200 µm diameters. The jetted steam is broken up into a series of droplets that can be deposited on flexible substrates. It can make controlled deposition of functional materials with suitable geometer on various substrates. In 2010, Madhusudan Singh *et al.* reported the developments in inkjet printing technology and its application including organic thin film transistors, light-emitting diodes, solar cells, conductive structures, memory devices, sensors, and biological/pharmaceutical tasks. Inkjet printing is a material-conserving deposition technique used for liquid phase materials. These materials or inks consist of a solute dissolved or otherwise dispersed in a solvent.

1.1 Principle of inkjet printing

Ink is ejected from a nozzle by applying a pulse of pressure to the fluid ink in the supply tube, upstream of that nozzle. There are two methods of creating this pressure pulse, thermal drop and piezoelectric drop.

Thermal drop was selected to use in this research based on principle as follows (see Figure 9). The droplets of ink are forced out of the nozzle by heating a resistor. The inside of ink channel is a resistor used to create a bubble. When electrical current is supplied to the resistor, heat can be generated and can cause enough to boil the ink. The ink closest to the resistor explosively boils, forming a vapor bubble and expanding. The expansion creates a pressure pulse in the fluid, causing ink in the nozzle (downstream of the heater) to be ejected toward the substrate. After, the vapor bubble cools and collapses. Then the surface tension of the ink meniscus in the nozzle pulls in more ink from the reservoir to refill the nozzle in preparation for the next drop to be ejected.

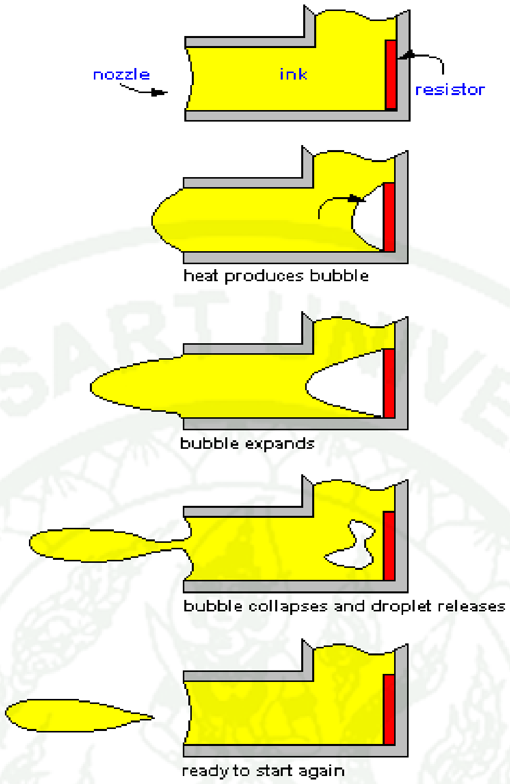

Figure 9 Principle of thermal inkjet printing.

Source: http://www.answers.com/topic/inkjet-printer-technology

The second pressure pulse technique uses piezoelectric materials which are crystalline materials having the property of deforming when high electric fields are applied (see Figure 10). An elastic diaphragm typically isolates the crystalline piezoelectric materials from the ink. With this principle, an electric pulse is passed through piezoelectric crystals or ceramic chambers. The run voltage causes a change in the shape of the ink chambers, whereby the ink is forced through the nozzles. The resulting vacuum in the chamber draws more ink from the ink tank and fill it up again. The ink channels in a piezoelectric ink jet print head can be formed using a variety of techniques, but one common method is lamination of a stack of metal plates, each of which includes precision micro-fabricated features of various shapes.

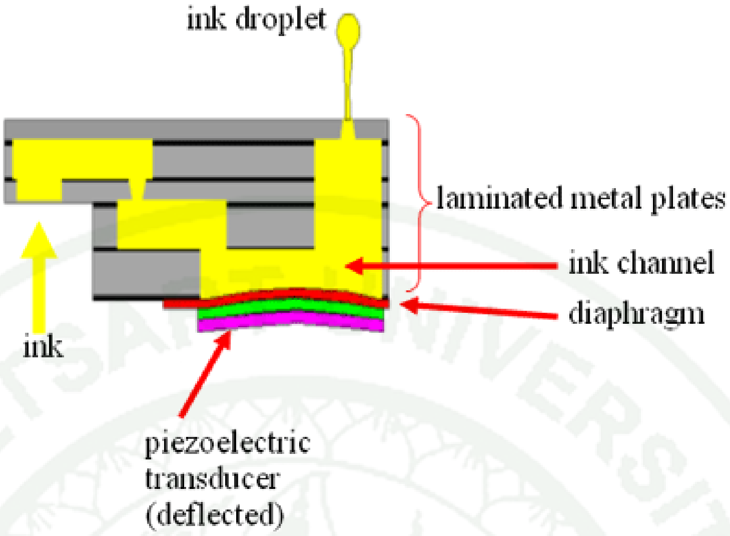

Figure 10 Principle of piezoelectric inkjet printing.

Source: http://www.imaging.org/ist/resources/tutorials/inkjet_printer.cfm

2. Conducting Polymers

Conducting polymers are organic polymers that conduct electricity. Such compounds may have metallic conductivity or semiconductors. Conducting polymers, such as polypyrrole (PPy), polyaniline (Pani), polythiophene (PTh), PEDOT and their derivatives, have been used as the active layers of gas sensors since early 1980s (Nylabder *et al.*, 1983). The most of the commercially available sensors are usually based on metal oxides and operated at high temperature. The sensors made of conducting polymers have many improved characteristics such as high sensitivities and short response time. Especially, it can work at room temperature. Moreover, conducting polymers are easy to be synthesized through chemical or electrochemical processes, and their molecular chain structure can be conveniently modified by copolymerization or structural derivations.

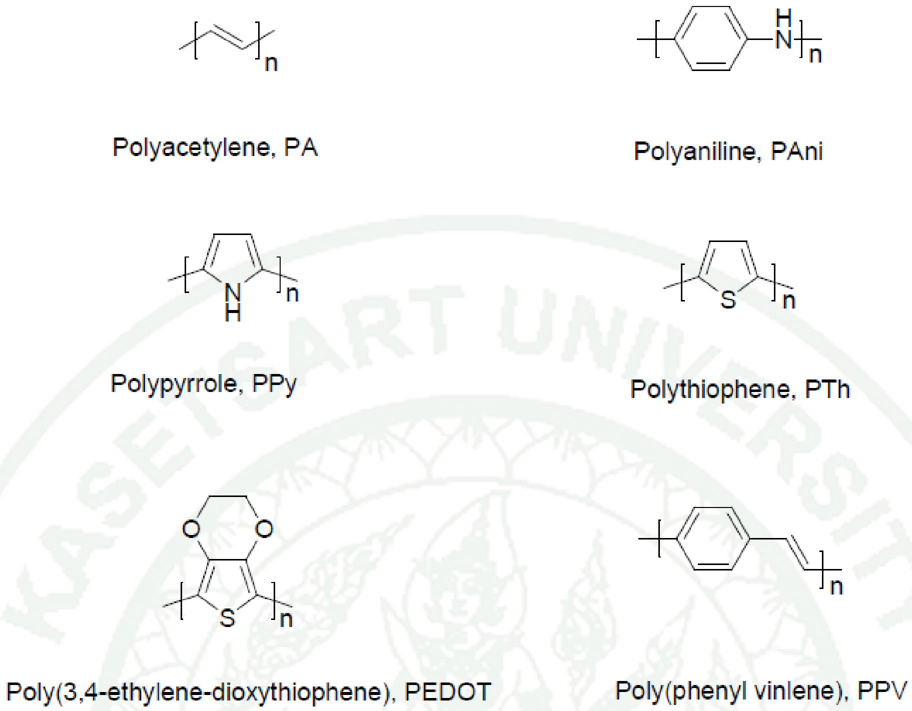

Figure 11 The scheme of several typical conducting polymers.

Source: Bai and Shi. (2007)

Figure 11 presents several typical conducting polymers used as the active layers in gas sensors. However, the conductivity of these pure conducting polymers are rather low ($<10^{-5}$ S cm^{-1}). In order to achieve highly conductive polymers, doping process is necessary.

Synthesis of conducting polymers, conducting polymers can be usually synthesized by chemical or electrochemical oxidizing the corresponding monomers. The electrochemical process of synthesizing a typical conducting polymer, such as the electrosynthesis of polythiophene in Boron trifluoride diethyl ether (BFEE), is demonstrated in Figure 12 (Shi *et al.*, 1995).

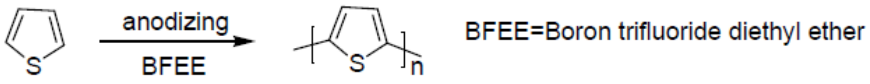

Figure 12 The scheme of electrosynthesis of Polythiophene in BFEE.

Source: Bai and Shi. (2007)

3. Poly(3,4-ethylenedioxythiophene) /poly(styrenesulfonate)

Poly(3,4-ethylenedioxythiophene) /poly(styrenesulfonate) or PEDOT:PSS is a polymer mixture of two ionomers. The chemical structures of PEDOT:PSS are shown in Fig. 13. One component in this mixture is made up of sodium polystyrene sulfonate which is a sulfonated polystyrene. Part of the sulfonyl groups are deprotonated and carry a negative charge. Poly(3,4-ethylenedioxythiophene) or PEDOT is a conjugated polymer and carries positive charges based on polythiophene. The charged macromolecules form a macromolecular salt (Groenendaal *et al.*, 2000). It is represents one such conjugated polymer that broadly used as the active material in flexible printed organic electronics because of its remarkably high conductivity, transparency, low redox potential, and relatively facile processability.

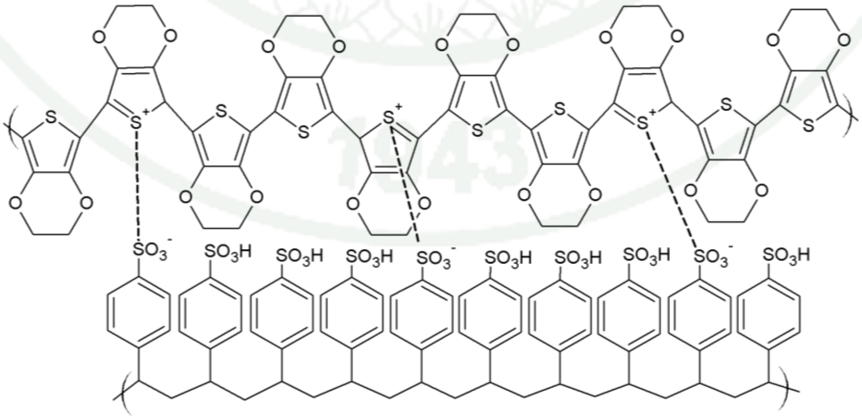

Figure 13 Schematic structures of PEDOT and PSS.

The conductivity of PEDOT:PSS can also be significantly improved by a post-treatment with various compounds, such as ethylene glycol (EG), dimethyl sulfoxide (DMSO). Which

DMSO can give the good conductivity and the low baselined resistance at room temperature (Kim *et al*., 2002), while the EG was added for improvement of the viscosity and surface tension (Mabrook *et al*., 2006).

4. Graphene material

Graphene is atom layer of carbon nanostructure in a densely packed honeycomb two-dimensional lattice (see Figure 14). It is the basic building block for other carbon nanomaterials, such as 0D fullerenes, 1D carbon nanotubes, and 2D nanographite sheets. Graphene has emerged as a highly important material for applications in nanoelectronics, flexible electronics, gas sensors and solar cells because high-quality graphene is strong, light, nearly transparent and an excellent conductor of heat and electricity.

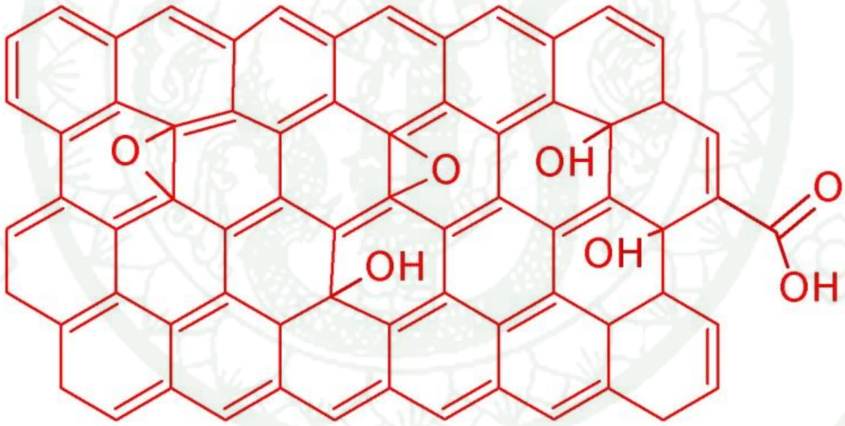

Figure 14 Schematic structures of graphene nanoplaletes (GNPs).

4.1 Synthesis of graphene material

Mechanical exfoliation: Mechanical exfoliation is a simple peeling process where a commercially available highly oriented pyrolytic graphite (HOPG) sheet was dry etched in oxygen plasma to many 5 μm deep mesa. The mesa was then stuck onto a photoresist and peeled off layers by a scotch tape. The thin flakes left on the photoresist were washed off in acetone and transferred to a silicon wafer. It was found that these thin flakes were composed of monolayer or a few layers of graphene (Novoselov *et al*., 2004).

Chemical vapor deposition (CVD): Chemical vapor deposition (CVD) on metal surfaces has been reported. Among them, the CVD growth appears to be the most promising technique for large-scale production of monolayer or few-layer graphene films. A typical CVD process (i.e. using Ni as a substrate) involves dissolving carbon into the nickel substrate followed by a precipitation of carbon on the substrate by cooling the nickel. The Ni substrate is placed in a CVD chamber at a vacuum of 10^{-3} Torr and temperature below 1000°C with a diluted hydrocarbon gas. The deposition process starts with the incorporation of a limited quantity of carbon atoms into the Ni substrate at relatively low temperature, similar to the carburization process. The subsequent rapid quenching of the substrate caused the incorporated carbon atoms to out-diffuse onto the surface of the Ni substrate and form graphene layers. Therefore, the thickness and crystalline ordering of the precipitated carbon (graphene layers) is controlled by the cooling rate and the concentration of carbon dissolved in the nickel which is determined by the type and concentration of the carbonaceous gas in the CVD, and the thickness of the nickel layer (Stankovich *et al*., 2007, May, 1996, Shelton *et al.,* 1974, Eizenberg *et al.*, 1979, Somani *et al*., 2006).

4.2 The study layer number of graphene sheet

Graphene can be described as a one-atom thick layer of graphite. The methods for determining the number of layers of graphene sheets including atomic force microscopy (AFM) and Raman spectra were normally used to identify the number of layers of graphene. Figure 15(a) shows the graphene sheet contains one, two, and three layers, as predetermined by AFM. Figure 15(b) shows the Raman spectra of graphene with different thicknesses, as well as that of highly ordered pyrolytic graphite (HOPG) for comparison. Figure 15(c) shows the Raman imaging of the G band intensity of the graphene sheets. The intensity of the G band along the dashed line is shown in Fig. 15(d). It can be clearly seen that the intensity of the G band increases almost linearly with the increase in graphene thickness. This can be used to determine the number of layers of multilayer graphene (Zhenhua *et al.*, 2008)

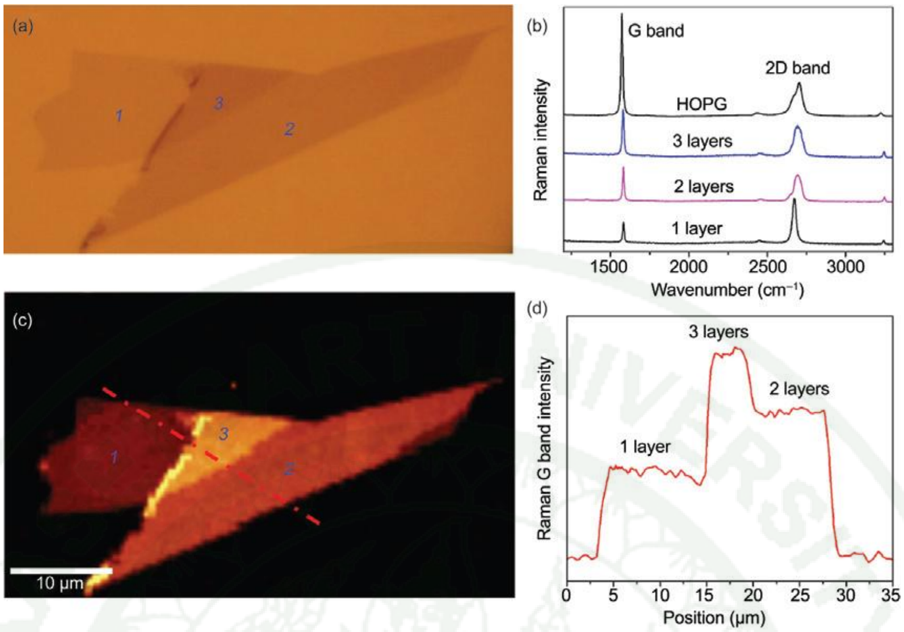

Figure 15 Optical image of graphene with 1, 2, and 3 layers (a). Raman spectra of graphene with 1, 2, and 3 layers as well as that of HOPG (b). Raman image plotted by intensity of the G band (c). The intensity cross-section of the Raman image corresponding to the dashed line in figure 4(c) (d).

Source: Zhenhua *et al.*. (2008)

4.3 Properties of graphene

Electronic properties: Graphene is a semi-metal or zero-gap semiconductor. One of the most useful properties of graphene is a zero-overlap semimetal (with both holes and electrons as charge carriers) with very high electrical conductivity. Carbon atoms have a total of 6 electrons; 2 in the inner shell and 4 in the outer shell. The 4 outer shell electrons in an individual carbon atom are available for chemical bonding, but in graphene, each atom is connected to 3 other carbon atoms on the two dimensional plane, leaving 1 electron freely available in the third dimension for electronic conduction. Experimental results from transport measurements show that graphene has a remarkably high electron mobility at room temperature, with reported values in excess of 15,000 cm$^{2}\cdot$V$^{-1}\cdot$s^{-1} (Geim and Novoselov, 2007) and theoretically potential limits of 200,000 cm$^{2}\cdot$V$^{-1}\cdot$s^{-1} (limited by the scattering of graphene’s acoustic photons) (Chen *et al*.,2008).

Mechanical propreties: Another of graphene standout properties is its inherent strength. Graphene is the strongest materials known with a breaking strength over 100 times greater than a hypothetical steel film of the same (thin) thickness (Lee *et al*.,2008), with a Young's modulus (stiffness) of 1 TPa (150,000,000 psi) (Braga *et al*.,2004). The spring constant of suspended graphene sheets has been measured using an atomic force microscope (AFM). Graphene sheets, held together by van der Waals forces, were suspended over SiO_2 cavities where an AFM tip was probed to test its mechanical properties. Its spring constant was in the range 1–5 N/m and the stiffness was 0.5 TPa, which differs from that of bulk graphite. These high values make graphene very strong and rigid. These intrinsic properties could lead to using graphene for Nanoelectromechanical system (NEMS) applications such as pressure sensors and resonators (Frank *et al*., 2007)

Optical Properties: Graphene is unique optical properties produce an unexpectedly high opacity for an atomic monolayer in vacuum, absorbing 2.3% of white light (Kuzmenko *et al*., 2008). Graphene band gap can be tuned from 0 to 0.25 eV (about 5 micrometre wavelength) by applying voltage to a dual-gate bilayer graphene field-effect transistor (FET) at room temperature (Zhang *et al*., 2009). The optical response of graphene nanoribbons is tunable into the terahertz regime by an applied magnetic field (Junfeng *et al*., 2008). Graphene/graphene oxide systems have exhibited electrochromic behavior, allowing tuning of both linear and ultrafast optical properties (Kurum *et al*., 2011).

MATERIALS AND METHODS

Materials

1) Canon PIXMA iX6560 and HP deskjet 2000 j210 printers
2) Electronic ink (PEDOT:PSS)
3) Graphene material
4) Paper photo and Transparency film (substrate)
5) Borosilicate glass chamber
6) Aluminium tape
7) Conductive silver paint
8) Digital Multimeter, Power supply
9) NI USB-6008 DAQ Card
10) Atomic force microscopy *(*AFM*)*
11) Scanning electron microscope (SEM)
12) Fourier transform infrared spectroscory (FTIR)
13) Raman spectroscopy
14) Transmission electron microscopy (TEM)
15) UV-visible spectrometer
16) Chemical (Dimethyl sulfoxide (DMSO), Ethylene glycol (EG), Triton x-100)

Methods

In this work, we have reported the fabrication of low-cost and flexible gas sensor using inkjet printing technique. The experiments can be divided into three steps; (I) preparation of electronic ink, (II) fabricate step of gas sensor, and (III) gas sensing measurement. The all details of experiment method will be discussed as follows;

1. Preparation of electronic ink

1.1 PEDOT:PSS ink

The PEDOT:PSS aqueous solution (Clevios™ P VP AI 4083, solid content 1.3–1.7%) was purchased from Heraeus Precious Metals GmbH & Co. KG. The PEDOT:PSS weight ratio is 1:6. The electronic ink was prepared based on the Poly(3,4-ethylenedioxythiophene) /poly(styrenesulfonate) (PEDOT/PSS). PEDOT:PSS was first dissolved in a mixture of solvents with a weight concentration of 89.82%. The solvent mixture contains 5.98 wt.% of dimethyl sulfoxide (DMSO), 3.99 wt.% of ethylene glycol (EG) and 0.199 wt.% of triton x-100. It should be noted that DMSO was used as the primary solvent that exhibits good conductivity and low baseline resistance at room temperature (Kim *et al.*, 2002), while EG and triton x-100 were added to improve of the viscosity and surface tension as well as to prevent of rapid drying and clogging in the printer head (Mabrook *et al.*, 2005). The final PEDOT:PSS solution was thoroughly stirred for 30 min at room temperature (see Fig. 16).

Figure 16 Preparation of electronic ink of PEDOT:PSS.

1.2 Graphene-PEDOT:PSS ink

For preparation of the graphene-PEDOT:PSS ink, the preparation of PEDOT:PSS ink have discussed in the above method. To prepare graphene solution, 10 mg of chemically synthesized graphene powder was dispersed in 5 ml of DMSO. The graphene powder was graphene nanoplatelets grade 3 (Cheap Tubes Inc.), which have specific surface areas of 600 – 750 m^2/g, an average thickness of 8 nm, conductivity of 7.813×10^3 Sm^{-1},and typical particle diameters of less than 2 µm. The graphene solution was then thoroughly sonicated for 30 min and stirred for 24 hr at room temperature. Next, graphene solution was mixed with 40 ml of PEDOT:PSS. To avoid agglomeration of graphene, PEDOT:PSS in designed chamber was placed in an ultrasonication bath (40 kHz) and graphene solution was gradually dripped into PEDOT:PSS with the rate of 25 µl/s. The final graphene-PEDOT:PSS solution (2.33 wt% of graphene to total solid content of PEDOT:PSS) was thoroughly sonicated for 30 min and stirred for 1 hr at room temperature (see in Fig. 17).

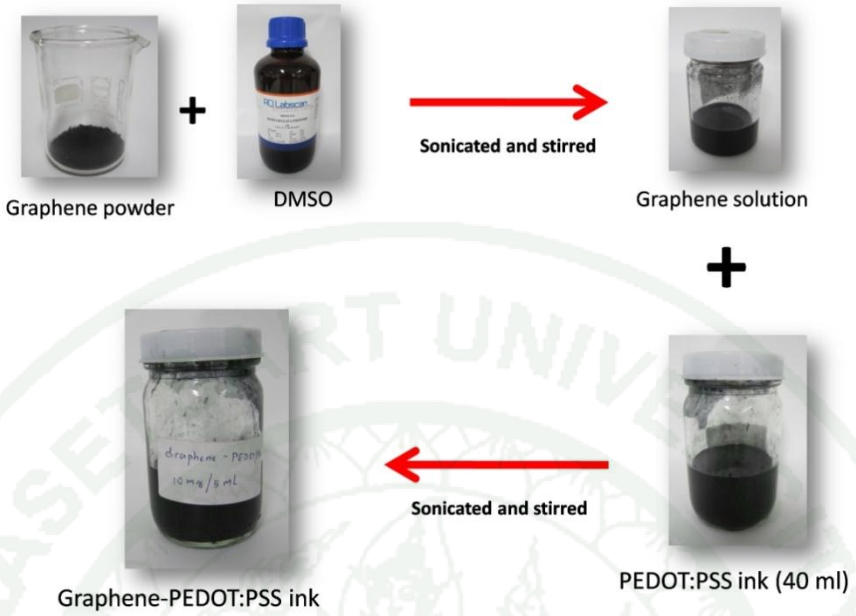

Figure 17 Preparation of electronic ink of graphene-PEDOT:PSS.

2. Fabrication of gas sensor

2.1 Design interdigitated electrodes by aluminum plate

A flexible gas sensor was fabricated by using modified Canon PIXMA iX4000 printer with a resolution (BW) of 4800×1200 dpi. The cartridge was refilled with the prepared electronic ink. A sensing film with rectangle geometry (1.5 cm×2.5 cm.) was directly printed on flexible substrate (Transparency film) (see Fig. 18a). The film thickness can be controlled by variation in the number of printed layers. The sensing films were printed from 1 to 10 layers (1 layer ~100 nm) (see Fig. 18b). The simple interdigitated electrodes made from patterned aluminum plate were attached on top of sensing films. The photograph of a fabricated gas sensor is shown in Fig. 18c

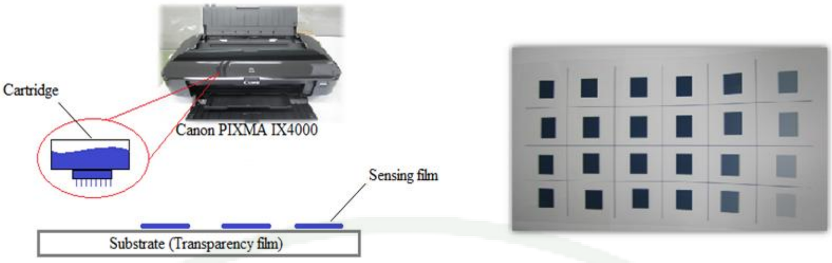

a. Ink-jet printing.

b. Sensing film on substrate (Transparency film).

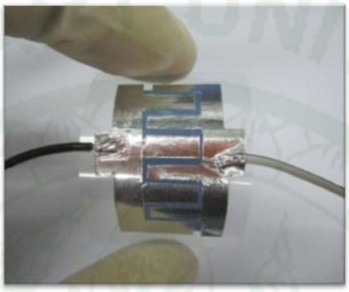

c. Photograph of a flexible gas sensor.

Figure 18 Gas sensor fabrication steps for the design interdigitated electrodes from aluminum plate.

2.2 The design interdigitated electrodes of silver conductive

For fabrication of flexible gas sensors, interdigitated electrodes with 1 mm interdigit spacing were deposited on a flexible substrate (Transparencies) by screen printing of silver conductive paste (see Fig. 19a-b). The prepared Graphene–PEDOT:PSS solution was then inkjet-printed over a rectangular electrode area of 1.5×2.5 cm^2 using modified HP deskjet 2000 j210 printer with a resolution (BW) of 1200×1200 dpi (see Figure 19b). The original ink in a printer cartridge was removed. The printer cartridge was thoroughly rinsed with DI water, dried with nitrogen gas and refilled with the prepared electronic ink. The thickness of inkjet-printed film could be controlled by varying the number of printed layers. The pristine PEDOT/PSS gas sensor was also fabricated and tested as a reference for comparison. The fabricated flexible graphene-PEDOT/PSS gas sensor is displayed in Figure 19d.

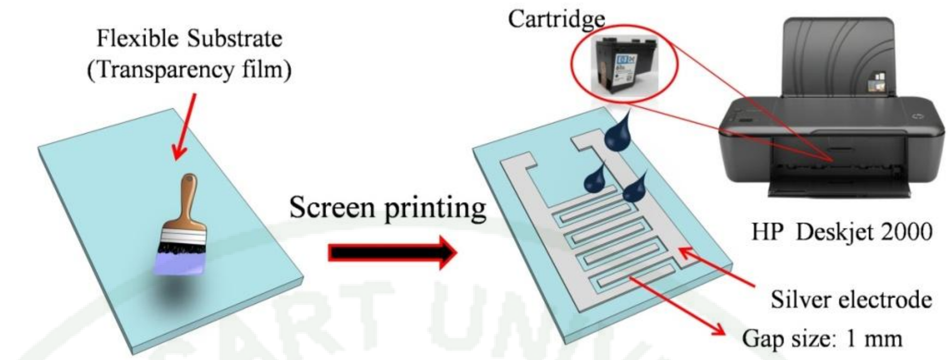

(a) Prepared interdigitated electrode. **(b) Ink-jet printing.**

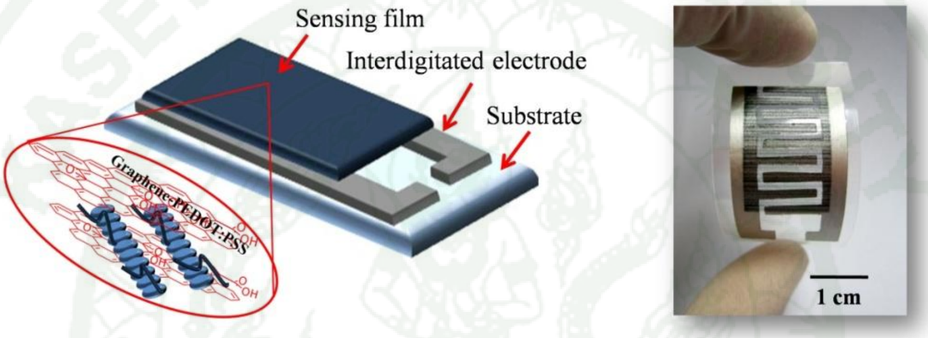

(c) Schematic diagram of gas sensor. **(d) Photograph of sensor device.**

Figure 19 Schematic diagram of gas sensor fabrication process for the design interdigitated electrodes from silver conductive.

3. Gas sensing measurement

The sensor resistances were measured in a borosilicate glass chamber at a constant applied voltage (10 V) using a simple voltage divider circuit. The response and selectivity of the sensors were then assessed by the standard flow-through method towards ethanol, methanol, toluene, acetone and NH_3 with gas concentrations ranging from 5 to 1000 ppm at room temperature. A constant flux of synthetic air of 2l/min was mixed with the target gas source at different flow rate ratios to desired concentrations using mass flow controllers. All experiments were performed at room temperature which was 26±2 °C and the relative humidity was 56±2%. Flexibility experiments were performed in which the sensors were bent to various degrees in exposure to NH_3. The bending angle was measured using a goniometer. The data were recorded every second using LabVIEW via a USB DAQ device for subsequent analyses.

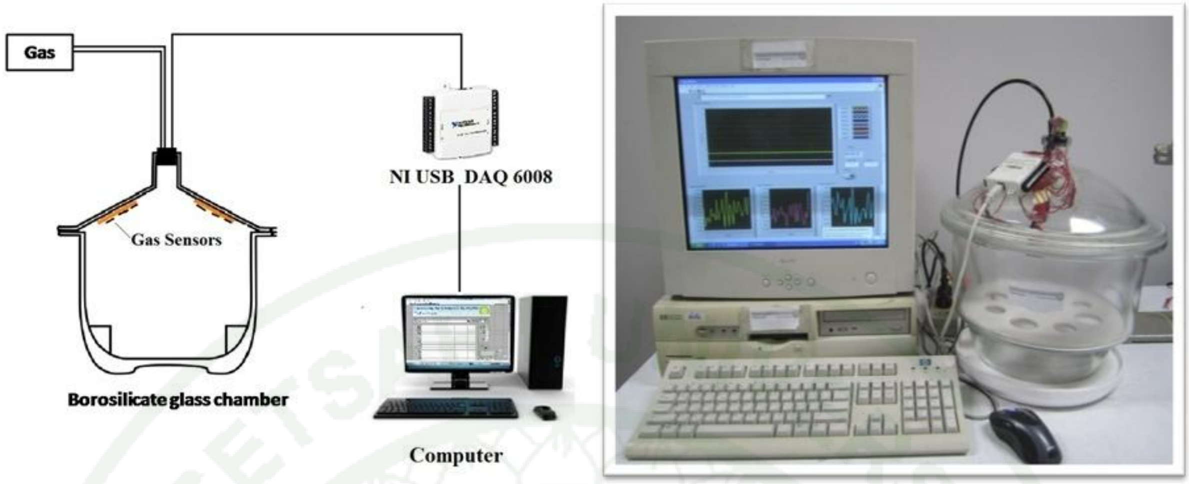

Figure 20 Photograph of gas sensing measurement.

RESULTS AND DISCUSSION

For result of experiment, we have studied the morphologies of flexible sensing films. The effect of thickness of sensing films and the optimum conditions of sensing films have been systematically investigated. Next, we have investigated the response and selectivity of flexible printed PEDOT:PSS and graphene-PEDOT:PSS gas sensors to various gases at room temperature.

1. Effect of thickness on sensing films.

AFM was used to investigate the surface morphology of PEDOT:PSS sensing film printed on flexible substrate (Transparency film) (See Fig. 21). The results indicate that the film surface is well uniform and only tiny defects are presented with a scan size area of 2 µm x 2 µm. The surface of inkjet printed film is rather smooth and continuous with the average surface roughness of ~ 7 nm.

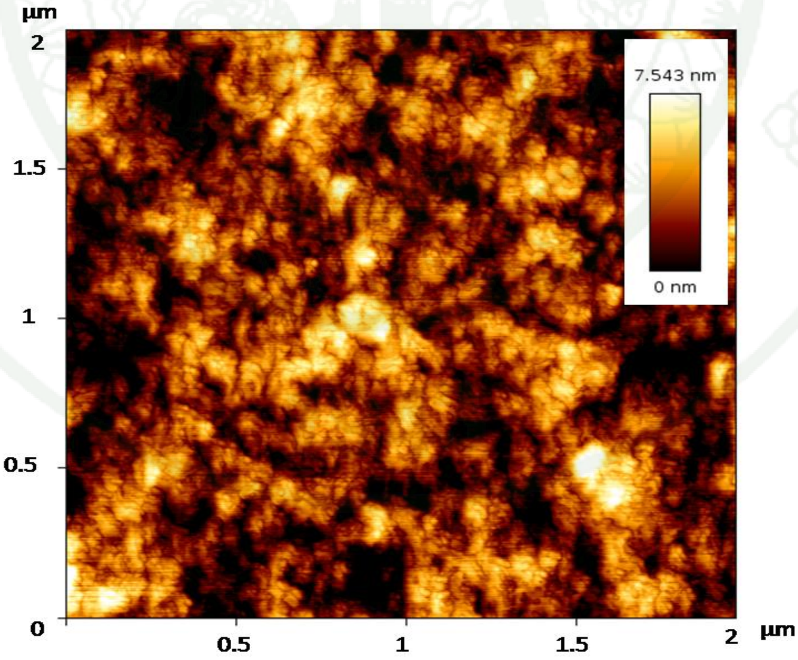

Figure 21 AFM images of an inkjet printed film of PEDOT/PSS on flexible substrate (Transparency film).

Fig. 22 shows the variation of the film resistance with sensing film thickness. The results indicate that the electrical resistance of the films decreases with increasing film thickness. The increase in film thickness can provide more charge carriers due to increase of conducting polymer molecules (PEDOT/PSS) between electrodes (Lee *et al*., 2004). These charge carriers make the contributions to the conductivity of the film resulting to decrease resistance with increasing film thickness.

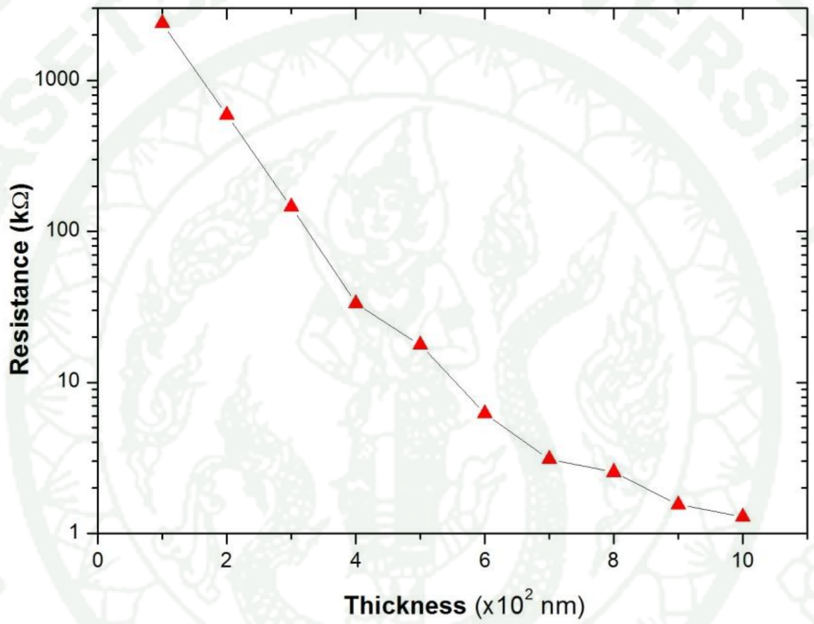

Figure 22 Relationship between the film resistance and sensing film thickness measured at room temperature.

In order to evaluate the sensing film stability, the resistance of each sensing film was re-measured weekly for 4 weeks. The results are displayed in Table 1. It shows that the resistances of all thickness films increase linearly from measurement at the first week to the fourth week. The increase in resistance depends on measurement period because the sensing polymer film is easily to absorb moisture of air that can make reduction of stable conductivity on sensing films. This sensor drift effect from humidity is a serious problem for polymer gas sensor. To overcome the obstacle, we have proposed a preheating process to refresh a sensor baseline resistance.

Table 1 Variation of resistances of sensing films versus time measured at room temperature.

Thickness ($\times 10^2$ nm)	1	2	3	4	5	6	7	8	9	10
1st Week (kΩ)	2380	590	145.05	33.32	17.72	6.21	3.09	2.54	1.55	1.28
2nd Week (kΩ)	3480	680	204.77	68.22	20.91	7.21	5.51	3.22	1.95	1.62
3rd Week (kΩ)	3670	830	376.00	90.08	29.32	7.73	5.92	4.57	2.37	2.04
4th Week (kΩ)	4030	981	439.00	95.10	32.04	9.92	6.29	4.91	2.63	2.24

The 200 nm thickness was selected for heating process study. The sensing film was heated with temperatures ranging from 50-130 °C for 20 min. The resistance of the sensing film was re-measured after film cool down to room temperature. The percentage change in resistance (ΔR) can be used to compare the efficiency of heating process. The ΔR is defined as $\Delta R\ (\%) = (R_{w1}-R_t)/R_{w1} \times 100$ where R_{w1} and R_t are the resistance measured at the first week and after the heating process, respectively.

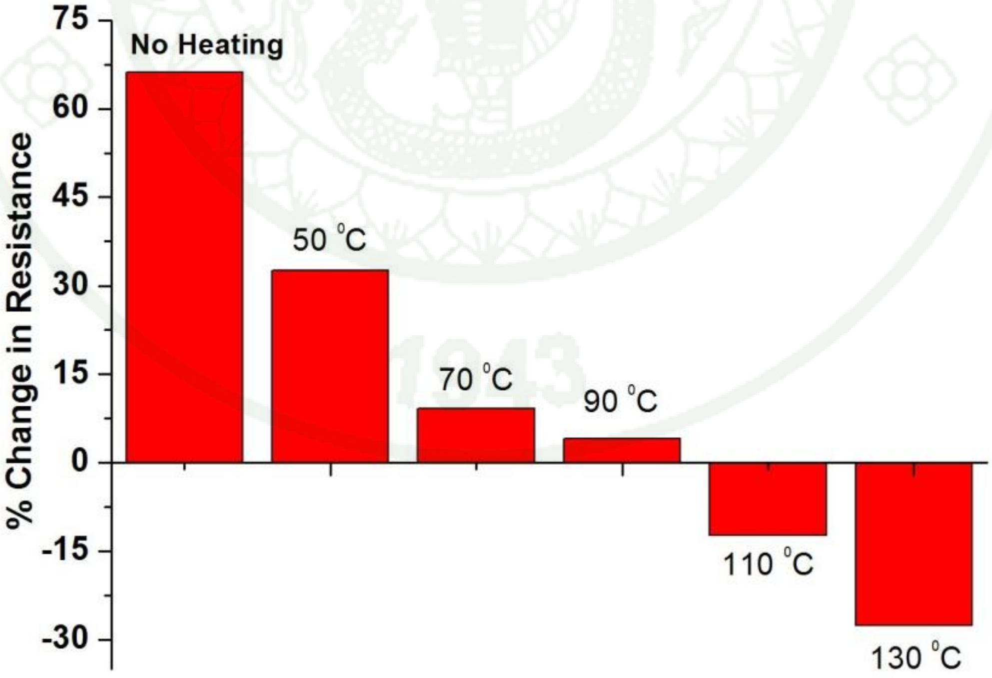

Figure 23 The percentage change in resistance of 200 nm thickness film after heating process (measurement at 4th week)

From fig. 23, it can be seen that the percentage change in resistance decreases with increasing heating temperature. The heating process removes moisture of air from sensing film. The temperature at 90 ^{0}c can make the resistance approach the 1st week resistance. However, to high heating temperature, the resistance of sensing film is lower that the 1st week resistance. Moreover, the high heating temperature may lead any cracks in sensing film and excessive distortion of flexible substrate (Transparency film).

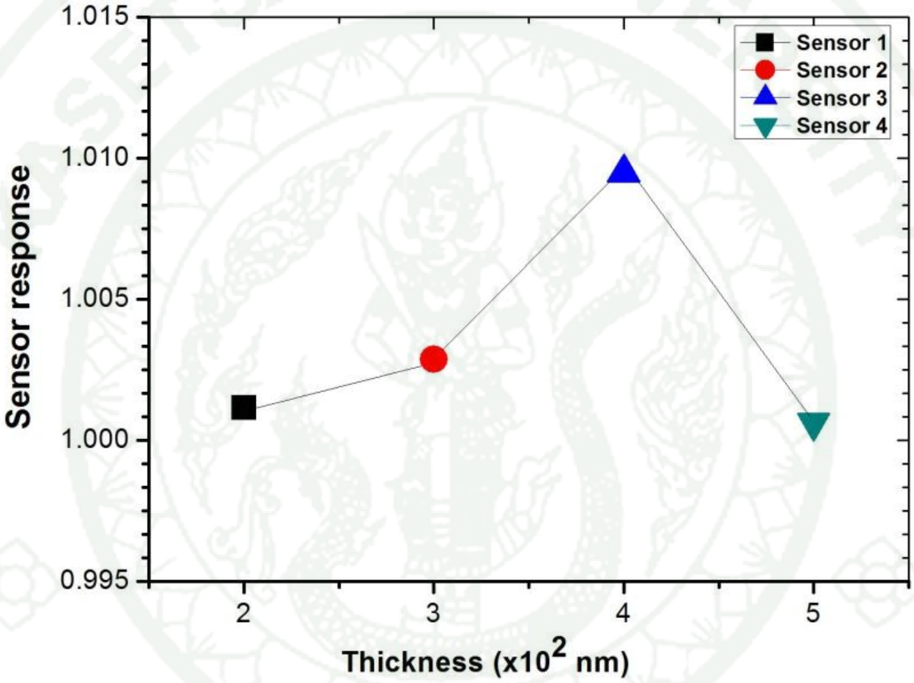

Figure 24 Sensor responses for ethanol concentration of 1000 ppm at room temperature for different film thickness gas sensors.

Four different thickness sensing films including 200 nm (Sensor 1), 300 nm (Sensor 2), 400 nm (Sensor 3), and 500 nm (Sensor 4) were selected for measurement of sensor response. All sensors were measured for ethanol concentration of 1000 ppm at room temperature. The sensor response (S) of the gas sensor is defined as $S= R/R_0$ where R_0 and R are the average resistance of the gas sensor in pure air and ethanol gas, respectively. From Fig. 24, it can be seen that the thickness of sensing film exhibits a strong response at thickness of 400 nm, and weaker responses at thickness of 200 nm, 300 nm, and 500 nm. It can be concluded that the flexible gas sensor exhibits high sensitivity to thickness of 400 nm (Sensor 3)

2. Graphene-PEDOT:PSS and PEDOT:PSS gas sensors

The flexible gas sensors of graphene-PEDOT:PSS and PEDOT:PSS sensing films were fabricated in step of the design electrodes of silver conductive. Sensing films of graphene-PEDOT:PSS and PEDOT:PSS were investigated to the characterization by using SEM, AFM, TEM, Raman, FTIR and UV-visible spectrometer. The flexible gas sensor have studied the behavior of the response and selectivity of flexible printed PEDOT:PSS and graphene-PEDOT:PSS gas sensors, which can be discussion as follow.

2.1 Characterization of sensing films

The thickness of inkjet-printed films was found to be increased approximately linearly with increasing printing number as shown in Fig. 25. The final thicknesses of pristine PEDOT/PSS and graphene–PEDOT:PSS sensing films are ~ 402 nm and ~ 407 nm, respectively.

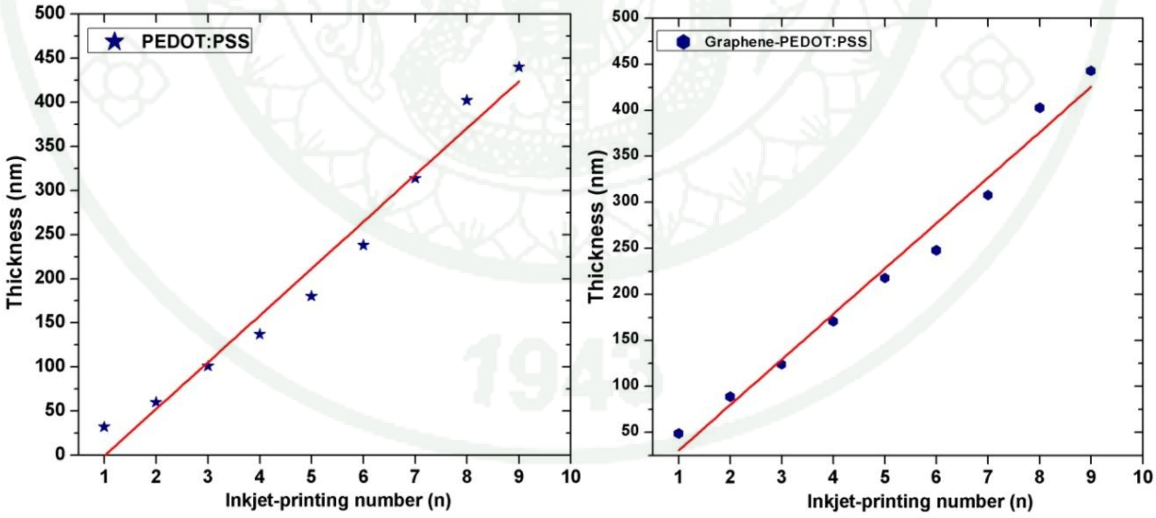

Figure 25 The thickness of (a) PEDOT:PSS and (b) graphene-PEDOT:PSS sensing films as a function of the inkjet-printing number.

Morphological characterization of the graphene-PEDOT:PSS composite film was performed by scanning electron microscope (SEM) measurements. Fig. 26 shows the SEM image of PEDOT:PSS and graphene-PEDOT:PSS films, respectively. It can be seen that pristine PEDOT:PSS film surface is very smooth (see Fig. 26a-b), the graphene-PEDOT:PSS composite film possesses a lot of clusters (see Fig. 26c-d).

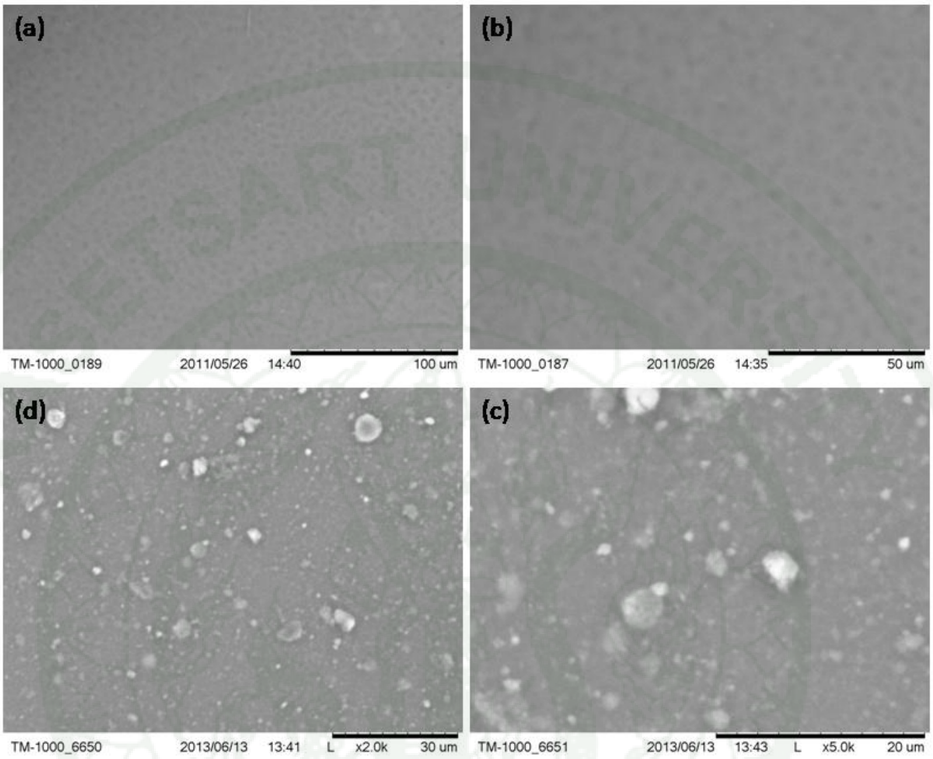

Figure 26 SEM image of an inkjet printed film of PEDOT:PSS(a-b) and graphene-PEDOT:PSS(c-d)

Surface morphologies and phase images of printed PEDOT:PSS and graphene-PEDOT:PSS sensing films were characterized by atomic force microscopy (AFM) with tapping mode as shown in Figure 27. From AFM images, it can be seen that pristine PEDOT:PSS film surface is very smooth containing only few tiny defects over a scan area of 10 μm x 10 μm (Figure 27a). With graphene inclusion, the film surface becomes relatively rough covering with a number of nanoprotrusions (Figure 27b). The nanoprotrusions have polygonal shapes with varying dimension in the range of ~50-1500 nm and hence should be corresponding to graphene nanosheets randomly embedded in PEDOT:PSS matrix. The average surface roughness of PEDOT:PSS and graphene-PEDOT:PSS are estimated to be ~2.73 nm and ~27.82 nm, respectively. The much larger surface roughness of graphene-PEDOT:PSS film suggests a significant enhancement of the active surface-area for gas adsorption by graphene (Yue *et al.*, 2013). From the AFM phase image (Figure 27c), the PEDOT:PSS sensing film shows relatively low contrast in the phase (0-20°). The bright and dark areas in the phase image are expected to correspond to PEDOT-rich grains and PSS-rich matrix, respectively. It is seen that the grain and matrix mixture is homogeneous indicating that PEDOT-rich grains exhibit very good connection with PSS-rich matrix via EG and DMSO binders resulting in the enhancement of carriers conducting pathways (Kim *et al*., 2011). In case of graphene-PEDOT:PSS (Figure 27d), the strong contrast in the phase (0-52°) can distinguish the relatively hard structures (graphene) from the softer component (PEDOT:PSS). However, the graphene structures in and on PEDOT:PSS network cannot be very clearly distinguished due to overcoating of PEDOT:PSS on graphene surfaces and limited resolution in AFM. Therefore, Raman spectroscopy will be used to confirm the existence of graphene in the sensing film.

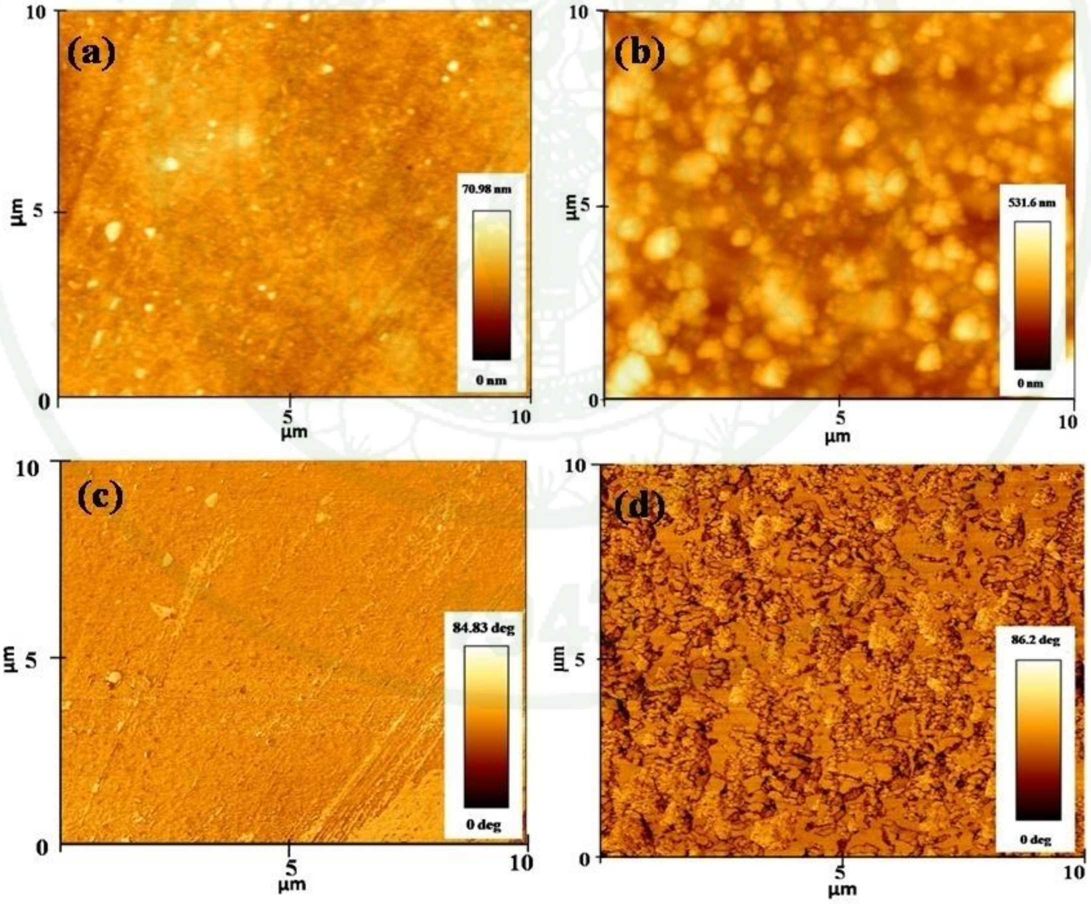

Figure 27 AFM topographical images of (a) PEDOT:PSS, (b) graphene-PEDOT:PSS and phase images of (c) PEDOT:PSS, (d) graphene-PEDOT:PSS sensing films.

The detailed structures of graphene solution and graphene dispersed in PEDOT:PSS were examined by transmission electron microscopy (TEM) as displayed in Fig. 28. Figure 28a shows a typical high resolution TEM image of the exfoliated graphene sheet in DMSO. It clearly shows visible crystal lattice fringes of the graphene structures with varying 3-6 sp^2-bonded carbon layers and DMSO does not make any effects on graphene structure. After mixing graphene into PEDOT:PSS, it can be seen that large polygon shapes are surrounded by smooth material as shown in Fig. 28b. The polygon shapes can be confirmed to be graphene by selected area electron diffraction (SAED) in the inset of Fig. 28b. The electron diffraction pattern is clearly visible, and the bright diffraction spots reflect to that of standard crystal graphite (Sriprajuabwong *et al.*, 2012, Nemade and Waghuley, 2013). Based on TEM and AFM results, formation of graphene-PEDOT:PSS nanocomposite can be explained by intercalated structure model (Kim *et al.*, 2012, Alexandre and Dubois, 2000). The graphenes were randomly embedded in PEDOT:PSS polymer matrix where PEDOT:PSS treads to coat on graphene surfaces while single extended polymer chain can be intercalated between the graphene layers leading to form hybrid multilayer morphology.

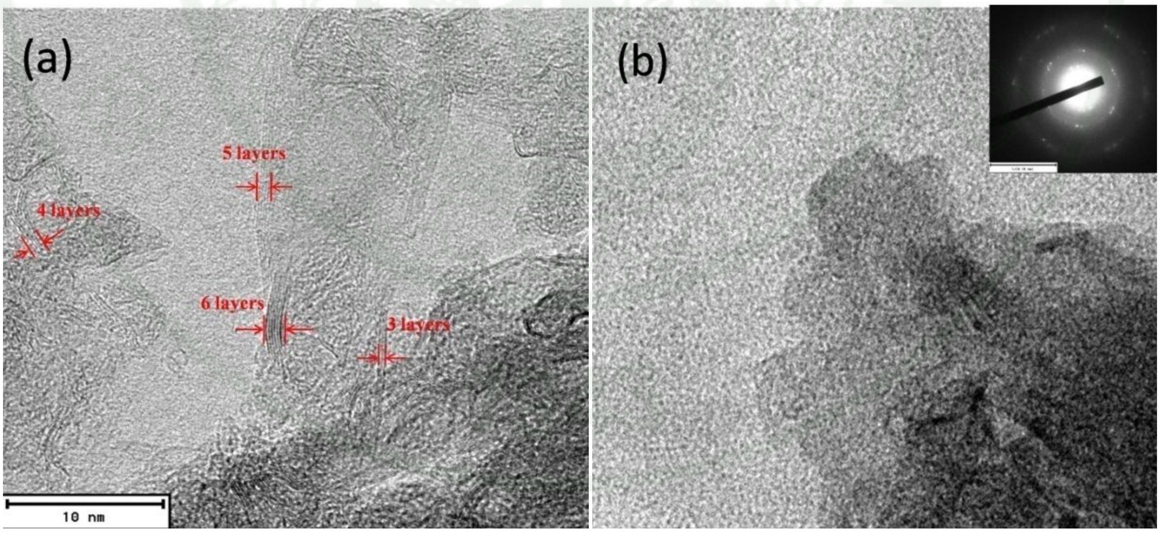

Figure 28 (a) High-resolution TEM image of graphene in DMSO and (b) typical bright field TEM image of graphene-PEDOT:PSS nanocomposite.

Raman spectra of (a) graphene-PEDOT:PSS and (b) PEDOT:PSS sensing films are shown in Figure 29. The characteristic peaks of PEDOT:PSS at 1116, 1418, and 1500 cm^{-1} are attributed to C-O-C deformation vibration, $C_\alpha=C_\beta$ symmetric stretching vibration, and asymmetrical stretching vibration of PEDOT:PSS chain structure, respectively (Xiong *et* *al*., 2013, Sakamoto et al., 2005, Farah *et al*., 2012, Barba *et al*., 2010). In case of graphene-PEDOT:PSS sensing film, carbon characteristic peaks at ~1335 cm^{-1} (D band), ~1574 cm^{-1} (G band) and ~2666 cm^{-1} (2D band) are pronounced while PEDOT:PSS peaks are almost vanished. The disappearance of PEDOT:PSS designates a strong $\pi-\pi$ interaction between graphene and PEDOT: PSS and the loss of coil conformation in PEDOT: PSS chain structure (Kim *et al*., 2012). The D peak represents either edge or lattice defects the while the G peak corresponds to primary sp^2-hybridized carbon bonds in graphene. The 2D band of graphene-PEDOT:PSS sensing film is related to zone boundary defects in graphene and can be used to indicate the number of sp^2 layers of graphene. The relatively broad 2D band of graphene compared with G band indicates that the existing graphene has a few sp^2 layers (Ni *et al*., 2008, Ferrari *et al*., 2006) corresponding to the TEM results.

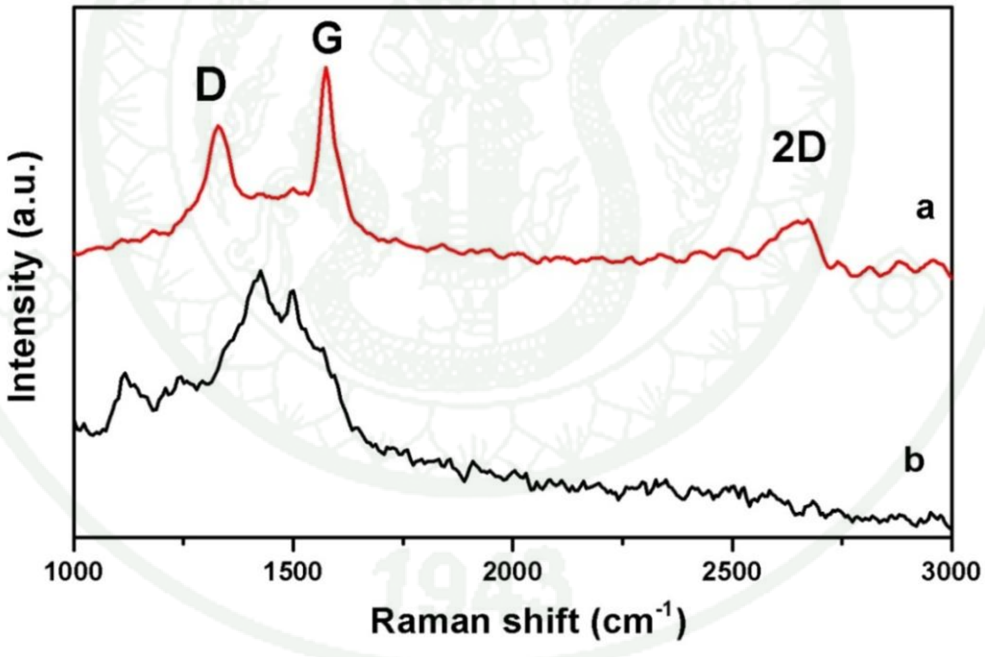

Figure 29 Raman spectra of (a) graphene-PEDOT:PSS and (b) PEDOT:PSS sensing films.

FTIR spectra of inkjet-printed graphene, PEDOT:PSS and graphene-PEDOT:PSS sensing films are illustrated in Fig. 30. In the FTIR spectrum of graphene, the peaks at 1095, 1224, 1338, 1412 and 1713 cm^{-1} are attributed to C-O contributions, C-OH stretching vibration mode, C–C stretching mode, O–H deformation vibration and C=O in the carboxyl stretching mode, respectively (Ghadim *et al*., 2013, Weng *et al*., 2014, Chu *et al*., 2012, Acik *et al*., 2010, Stankovich *et al*., 2006). These results suggest that the graphene contains carboxylic acid, carbonyl moieties and hydroxyl functional groups after treatment in DMSO according to the schematic structure of graphene in Fig. 14. In case of the spectra of PEDOT:PSS and graphene-PEDOT:PSS sensing films, they contain similar peaks of S–phenyl bond in sulfonic acid at 1010, 1039, and 1060 cm^{-1}, C-O-C stretching vibration peak at 1263 cm^{-1} and C-S bond in the thiophene ring at 705, 858, and 946 cm^{-1} (Sriprajuabwong *et al*., 2012, Karuwan *et al*., 2012). In addition, C=C stretching vibrations peak of the thiophene ring at 1521 cm^{-1} and C-O bonding peak at 1126 cm^{-1} for PEDOT:PSS are slightly shifted to 1519 cm^{-1} and 1120 cm^{-1} for graphene-PEDOT:PSS. The small red shift in FTIR spectra of graphene-PEDOT:PSS sensing film could be due to the delocalization of electrons from aromatic rings and C-O bonds to the π-clouds of graphene (Mandal *et al*., 2012). This suggests the presence of $\pi-\pi$ interactions between graphene and PEDOT: PSS which is in agreement with the UV- visible absorption spectra as shown in Fig 31. Moreover, graphene-PEDOT:PSS exhibits an extra C=O carbonyl stretching peak at 1743 cm^{-1}, indicating the successful formation of hybrid graphene-PEDOT:PSS sensing film (Si *et al*., 2012). However, the exact position for π -network construction in hybrid graphene-PEDOT:PSS composite still needs to be intensively studied *based on* high level quantum chemical calculations.

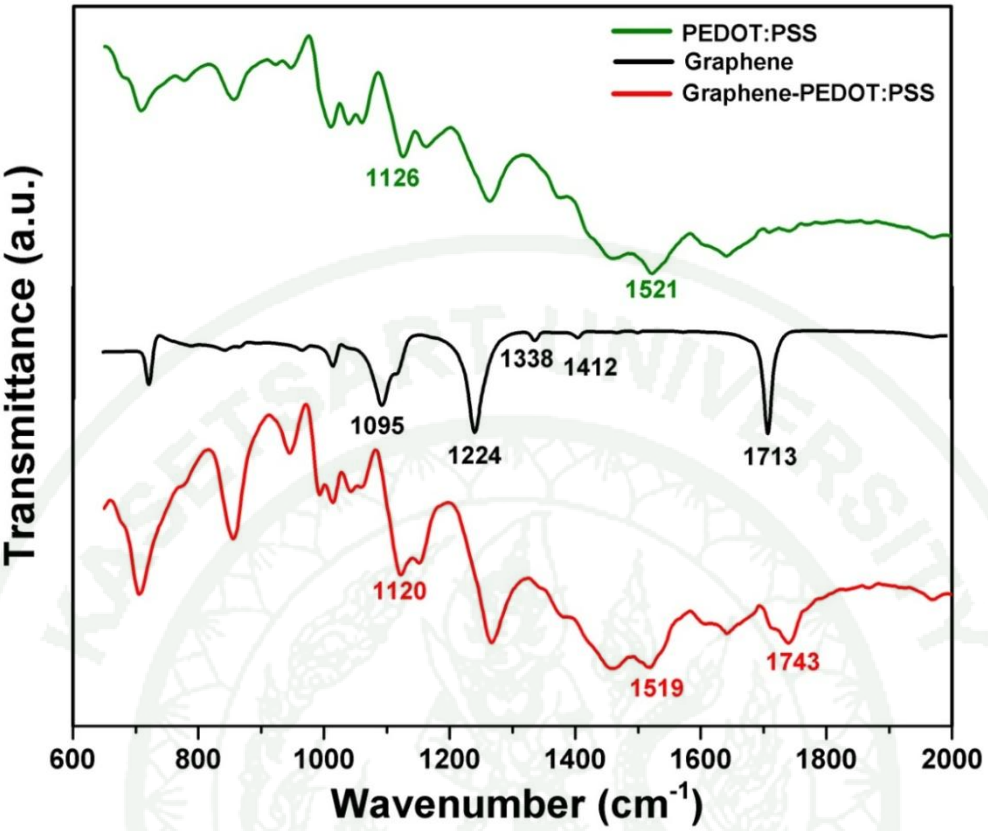

Figure 30 FTIR spectra of PEDOT:PSS, graphene and graphene-PEDOT:PSS sensing films.

The UV-visible spectrometer (Lambda 650 Perkin Elmer) was used to study the π-π^* transitions in graphene and PEDOT:PSS. The UV-visible spectra of graphene, PEDOT:PSS and graphene-PEDOT:PSS composite are shown in Fig. 31. A broad absorption peak (centered at ~ 268 nm) of graphene is attributed to the π-π^* transitions of aromatic C–C bonds (Ricardo *et al*., 2014). In case of PEDOT:PSS, the UV-vis absorption spectrum exhibits two peaks at 254 nm and 260 nm corresponding to typical absorption bands from the aromatic ring of PSS (Sun *et al.*, 2012). In case of graphene-PEDOT:PSS composite, the absorption peaks are located at 254 and 260 nm which red shifted and appeared a broad absorption peak of graphene. These results suggest the formation of graphene into the PEDOT:PSS composite and π – π electron donor–accepter interaction between graphene and PEDOT:PSS (Trang *et al*., 2012).

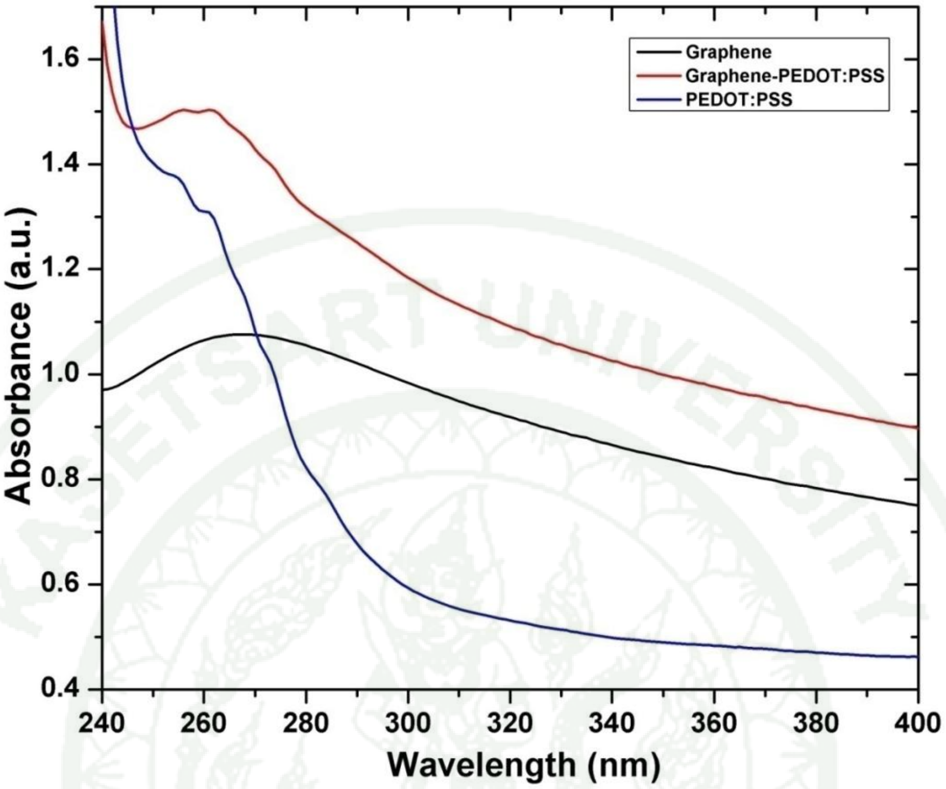

Figure 31 UV- visible spectra of graphene, PEDOT:PSS and graphene-PEDOT:PSS composite.

2.2 Gas Sensing Properties

Figure 32 shows the dynamic responses of the flexible printed PEDOT:PSS and graphene-PEDOT:PSS gas sensors towards 500 ppm of NH_3 at room temperature. It indicates that the sensor exhibits good repeatability of response towards repeated NH_3-sensing cycles at room temperature. The resistances of both sensors increase upon exposure to NH_3 and recover to the initial value upon the removal of NH_3 in air. The resistance changing behaviors may be attributed to the adsorption and desorption of NH_3 molecules and swelling mechanism of the sensing films. The details of sensing mechanism for graphene-PEDOT:PSS gas sensor will be discussed in the next section.

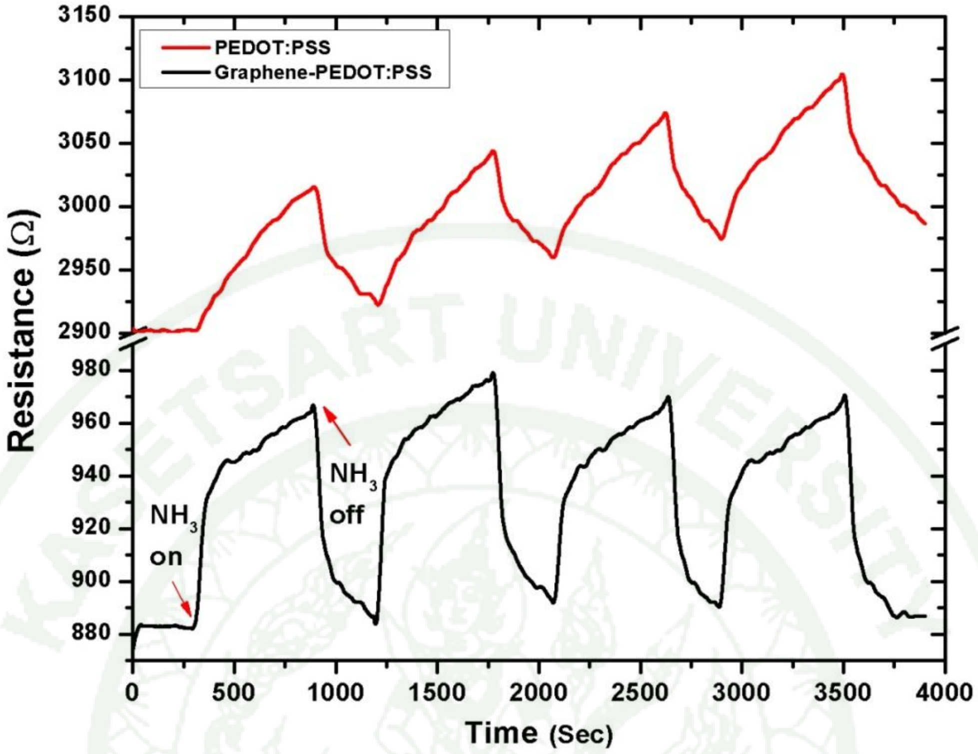

Figure 32 Dynamic responses of the flexible printed PEDOT:PSS and graphene-PEDOT:PSS gas sensors to 500 ppm NH_3 at room temperature.

In addition, it can be observed that graphene-PEDOT:PSS gas sensor has much lower initial resistance than pristine PEDOT:PSS. The conductivities of PEDOT:PSS and graphene-PEDOT:PSS sensing films based on 4-point probe measurements at a constant applied current (10 nA) are 1.580×10^2 Sm^{-1} and 1.755×10^2 Sm^{-1}, respectively. It refers increase of charge carrier concentration due to graphene incorporation. The response time, defined as the time to reach 90% of the maximum total resistance change, of the flexible printed PEDOT:PSS and graphene-PEDOT:PSS gas sensors are estimated to be ~6 min and ~3 min, respectively. Moreover, the resistance of graphene-PEDOT:PSS gas sensor could recover almost completely to the initial value within the pure air exposure times of 5 min while the PEDOT:PSS gas sensor shows undesirable resistance drift. Thus, graphene-PEDOT:PSS gas sensor exhibits relatively short response and recovery times compared with PEDOT:PSS one. The slower response and recovery of PEDOT:PSS gas sensor may be due to low diffusion and short penetration depth of gas molecules on very smooth surface of the PEDOT:PSS sensing film.

In order to investigate the response and selectivity of flexible printed PEDOT:PSS and graphene-PEDOT:PSS gas sensors, these sensors were exposed to a variety of volatile organic compounds (VOCs) including NH_3, diethylamine, acetone, ethanol, methanol and toluene at concentrations ranging from 5 ppm to 1000 ppm at room temperature. The response characteristic is then analyzed from the percentage change of the gas response defined as $S(\%) = [(R_{gas} - R_{\mathrm{air}}) \times 100]/R_{\mathrm{air}}$, where R_{air} and R_{gas} are the resistance of sensor in pure air and in test gas, respectively as demonstrated in Fig. 33. It can be seen that the flexible pristine PEDOT:PSS gas sensor shows relatively high response to NH_3 compared with diethylamine, acetone, ethanol, toluene, and methanol at room temperature (See Fig 33a). At 1000 ppm concentration, the percentage change of the gas response of PEDOT:PSS gas sensor to NH_3, diethylamine, ethanol, acetone, toluene and methanol are 6.9%, 5.9%, 3.2%, 2.8%, 2.1% and 1.9%, respectively. At low concentration (5-50 ppm), PEDOT:PSS is still able to response to NH_3 with the gas response ranging from 0.9 - 3.7 % as shown in inset of Fig. 31a.

With graphene addition, the gas response and selectivity to NH_3 are substantially improved as seen in Fig. 33b. The graphene-PEDOT:PSS gas sensor exhibits a remarkably high response to NH_3 but is almost insensitive to acetone, ethanol, toluene and methanol at the concentration range of 5-1000 ppm. At 1000 ppm of NH_3, the gas response of graphene-PEDOT:PSS sensor are 18.9% which is almost 3 times as high as that of PEDOT:PSS gas sensor. At low concentration (5-50 ppm), the gas response of graphene-PEDOT:PSS gas sensor to NH_3 is still higher than that of undoped one with the gas response ranging from 1.2 - 5.5 % as shown in inset of Fig. 33b. However, at the concentration range (5 and 10 ppm), the gas response of graphene-PEDOT:PSS gas sensor to NH_3 and diethylamine are not significant different. The detection limit of NH_3 for graphene-PEDOT:PSS sensor is estimated to be <10ppm at the room temperature. It should be noted that the NH_3 and diethylamine have the similar amines functional group and possess lone electron pairs. Therefore, diethylamine can be used to confirm a high selectivity of graphene-PEDOT:PSS gas sensor to NH_3 with concentration > 25 ppm at room temperature.

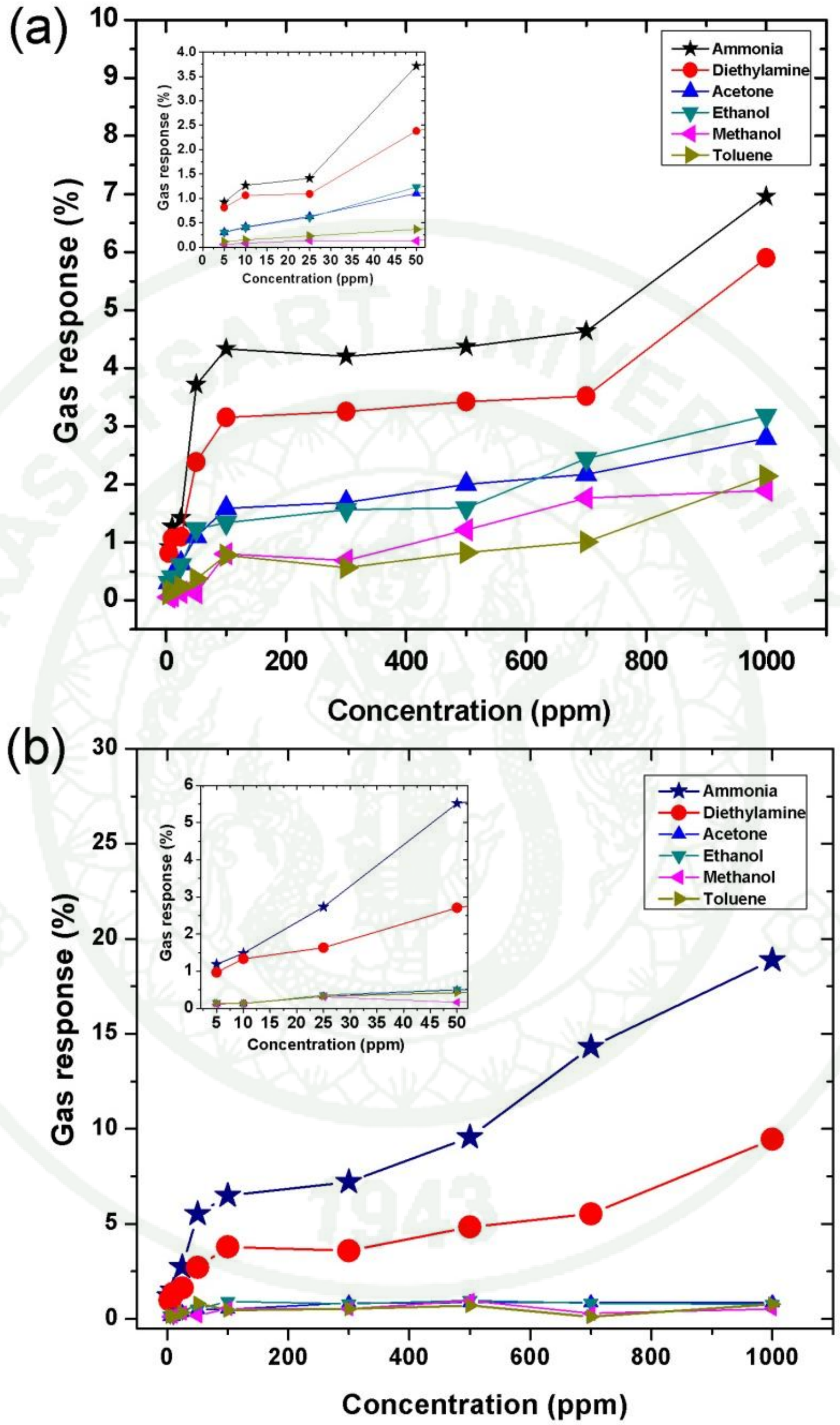

Figure 33 Gas responses of (a) PEDOT:PSS and (b) graphene-PEDOT:PSS gas sensors to various concentrations of different VOCs at room temperature

Enhanced NH_3 sensing properties of graphene-PEDOT:PSS gas sensor may be attributed to the (I) increase of the surface roughness as shown in Fig 27, (II) intrinsic sensing properties of graphene and (III) π-electron interaction by graphene loading in sensing film. (I) the gas sensitivity is directly proportional with the surface roughness of sensing film due to provide a specific surface-to-volume ratio (Suchea *et al.*, 2006). The much larger surface roughness of graphene-PEDOT:PSS film therefore enhances the active surface-area for gas adsorption. (II) It is well-known that graphene under ambient conditions behaves as p-type semiconductor that induce a hole-like carrier concentration (Romero *et al.*, 2009) while NH_3 is an electron donor. When graphene-based sensor is exposured to NH_3, depletion of holes from the valence band of graphene occurs resulting in an increase in resistance. Thus, mixture of graphene to PEDOT:PSS increases NH_3 sensitivity. (III) The NH_3 molecules may interact not only to graphene and PEDOT:PSS but also π- π interaction between graphene and PEDOT:PSS (Huang *et al.*, 2012). In the exposure of the polar molecule, i.e NH_3, it can induce charge-transfer mechanisms across delocalized π-electrons resulting to improve the sensing performance. As results, graphene-PEDOT:PSS sensor therefore exhibits high response and selectivity to NH_3 over pristine PEDOT:PSS sensor.

The effect of flexibility on NH_3 sensing of graphene-PEDOT:PSS and PEDOT:PSS sensors was investigated by varying the bending angle (ϴ) from 10° to 70° with the exposure of 500 ppm NH_3 as shown in Fig. 34. Response deviation (ΔS) is defined as $\Delta S = S_\theta - S_0$, where S_θ and S_0 are the gas response of sensor with bending angle (ϴ) and bending angle of 0 degree, respectively. It is interesting that the gas response of both sensors on NH_3 sensing increases when the bending angle increases. At bending angle of 70°, the response of graphene-PEDOT:PSS and PEDOT:PSS sensors on 500 ppm NH_3 increase from 9.6 % to 15.8 % (+ 6.2 %) and from 4.4% to 9.7 (+5.3%) respectively. Increasing of sensing properties by bending angle may come from contribution of swelling mechanism process that NH_3 molecules can easily diffuse into the polymer chains matrix. This purpose is in agreement with an increase in initial based line resistance of sensor after bending.

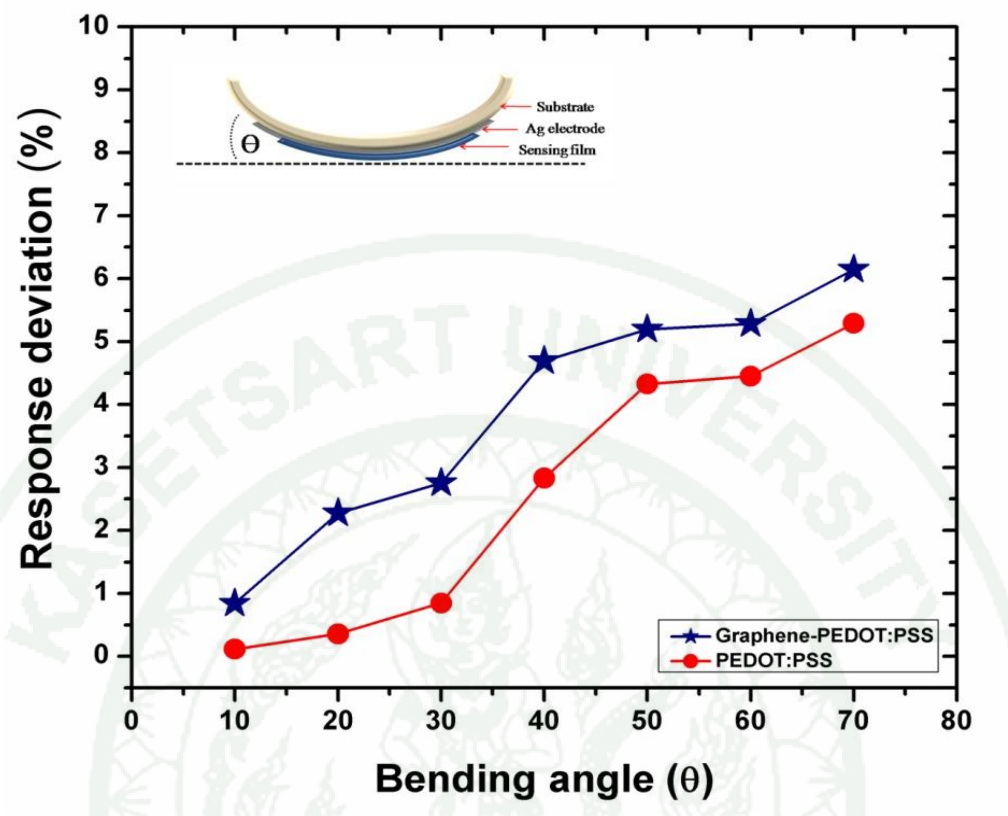

Figure 34 Flexibility of PEDOT:PSS and graphene-PEDOT:PSS gas sensors in response of 500 ppm NH_3 at room temperature.

The flexible printed graphene-PEDOT:PSS gas sensor has been stored at room temperature with a relative humidity of 56±2% more than 6 months. The sensor has been tested with exposure of 500 ppm NH_3 every week. The average monthly gas response of the flexible printed graphene-PEDOT:PSS gas sensor to 500 ppm NH_3 as the function of time is displayed in Figure 35. The sensor shows the long-term stability up to 3 months. The response of flexible printed graphene-PEDOT:PSS gas sensor still maintained 88.58% of its original response to 500 ppm NH_3.

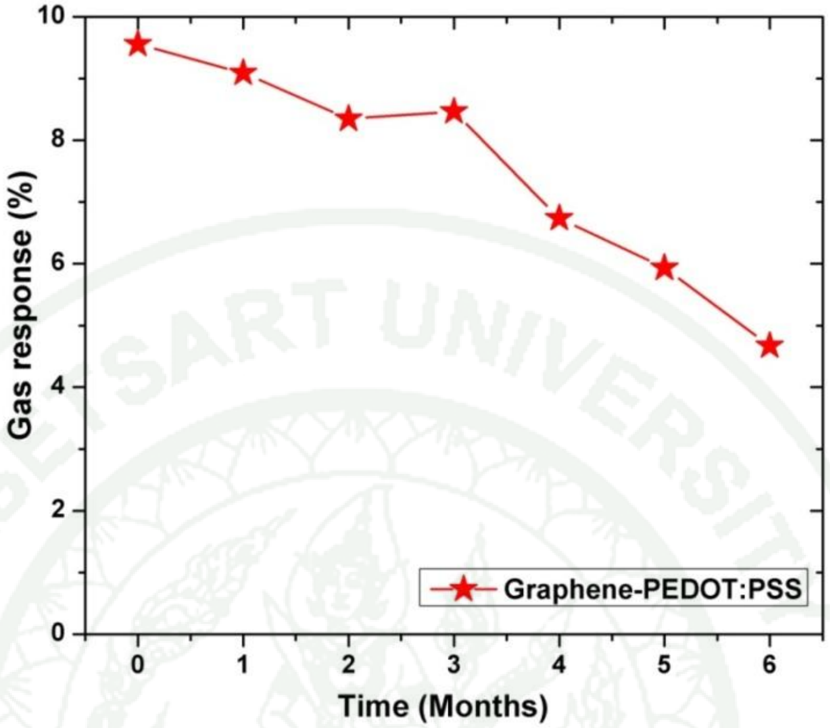

Figure 35 Stability of graphene-PEDOT:PSS gas sensor response to 500 ppm NH_3 during 6 months.

Figure 36 shows the Effect of graphene content on the response of the graphene-PEDOT:PSS sensor to 500 ppm NH_3 at room temperature. The printed graphene-PEDOT:PSS composite sensing film contains the 2.33 wt% of graphene to total solid content of PEDOT:PSS. The weight ratio of graphene to PEDOT:PSS was varied such as 0.12 wt% (0.5 mg),0.23 wt% (1 mg), 0.70 wt% (3 mg), 1.16 wt % (5 mg), 1.63 wt% (7 mg), and 2.33 wt% (10 mg). It can be found that the amount of graphene doping to composite sensing film directly affects on the NH_3 response. The gas response to 500 ppm NH_3 at room temperature increases with increasing graphene content. However, high graphene content in electronic ink usually causes the clogging problem in the printer head and inhomogeneous printed sensing film.

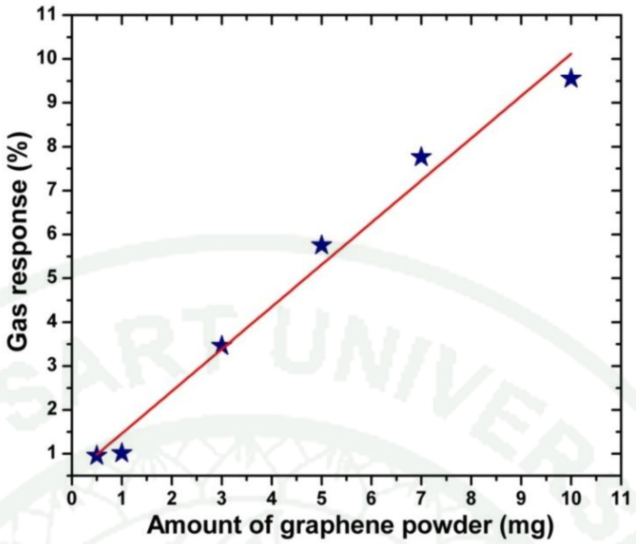

Figure 36 Effect of graphene content on the response of the graphene-PEDOT:PSS sensor to 500 ppm NH_3 at room temperature.

The graphene, PEDOT:PSS, and graphene-PEDOT:PSS gas sensors have been investigated to 500 ppm NH_3 at room temperature. A comparison of gas response is displayed in Fig. 37. The gas responses of graphene-PEDOT:PSS, PEDOT:PSS and graphene gas sensors are 9.553%, 4.371%, and 2.383%, respectively. It can be seen that the sensing function of graphene is too low.

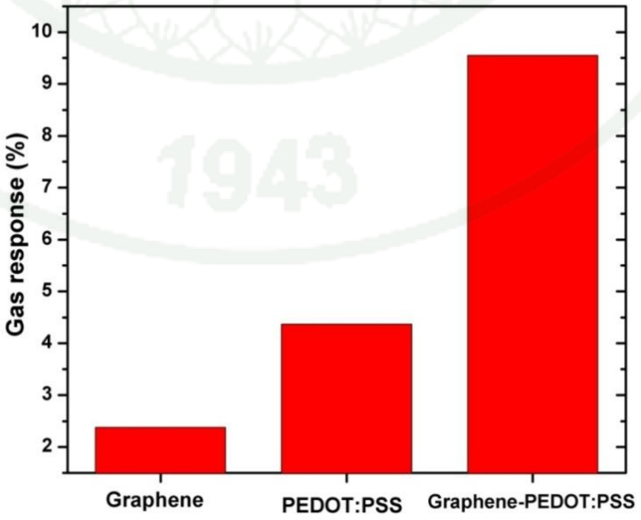

Figure 37 A comparison of gas responses of graphene, PEDOT:PSS, and graphene-PEDOT:PSS gas sensors to 500 ppm NH_3 at room temperature.

2.3 Sensing mechanism of graphene-PEDOT:PSS sensor of ammonia gas

Several sensing mechanisms have been proposed for the conducting polymer systems including redox reactions between the polymer and analyte, charge transfer between the polymer and analyte and polymer swelling (Lina *et al.*, 2009, Bai and Shi, 2007). In this case, the resistance of graphene-PEDOT:PSS increases upon NH_3 exposure and decreases to its initial based line in pure air. This resistance changing behavior may be explained based on three possible mechanisms:

(I) Reducing reaction between NH_3 and chemisorbed oxygen $(O_2(ads) + e^- \rightarrow O_2^-(ads))$ on the p-type graphene-PEDOT:PSS surface. It should be noted that oxygen in the reversible low-temperature (< 100 °C) chemisorption participates as O_2^- (Weber, 1970). O_2^- may be trapped at the surface of graphene-PEDOT:PSS sensing film in dry air before NH_3 exposure. When NH_3 molecules directly adsorb on the surface, it reacts with the oxygen species and gives electrons back to graphene-PEDOT:PSS surface according to the reaction : $4NH_3(gas) + 5O_2^-(ads) \rightarrow 4NO(gas) + 6H_2O(gas) + 5e^-$ (Gautam and Jayatissa, 2012). The transferred electrons in conduction band recombine with holes from valence band resulting in lower carrier concentrations and higher resistance of the p-type graphene-PEDOT:PSS sensing film. However, chemisorbed oxygen is less dominated to the sensing mechanism of graphene-PEDOT:PSS film at room temperature.

(II) Direct charge transfer process between NH_3 molecules and graphene-PEDOT:PSS surface. When NH_3 molecules are adsorbed on the graphene-PEDOT:PSS surface by physisorption, the holes of conductive graphene-PEDOT:PSS will interact with the electron-donating NH_3 analyte (Wu *et al.*, 2013). The delocalization degree of conjugated π electrons of sensing film is increased by charge transfer from the adsorbed NH_3 molecules. This leads to the formation of a neutral polymer backbone and decrease in charge carriers resulting in the decrease of the electrical conductivity of the sensing film (Kwon *et al.*, 2010, Jian *et al.*, 2013). Moreover, the addition of graphene to into PEDOT:PSS increases specific adsorption surface area and π- π interactions.

(III) Swelling process from the diffusion of NH_3 molecules into the graphene/polymer chains matrix. In PEDOT:PSS sensing films, a single PSS chain interacts electrostatically over its length with many shorter PEDOT chains, which tend to have short interchain distance (Crispin *et al.*, 2003). Thus, the electron hopping process prefers to occur between PEDOT chains. When NH_3 molecules diffuse into polymer matrix, electron hopping process becomes more difficult because the PEDOT interchain distance increases due to the swelling process. In the case of graphene-PEDOT:PSS sensor, graphene embedded into polymer matrix acts as conductive pathways that favor the hopping of electrons. The swelling process can cause the graphene to stay apart, disrupting conductive pathways in the sensing film. The increase of PEDOT distance and decrease of graphene's conductive pathways occur simultaneously, leading to significant increase in resistance of the graphene-PEDOT:PSS sensor upon NH_3 exposure and therefore enhanced NH_3 response. The resistance of graphene-PEDOT:PSS sensor will recover to its base line after polymer shrinks back into the initial volume by NH_3 out-diffusion via the purge of dry air.

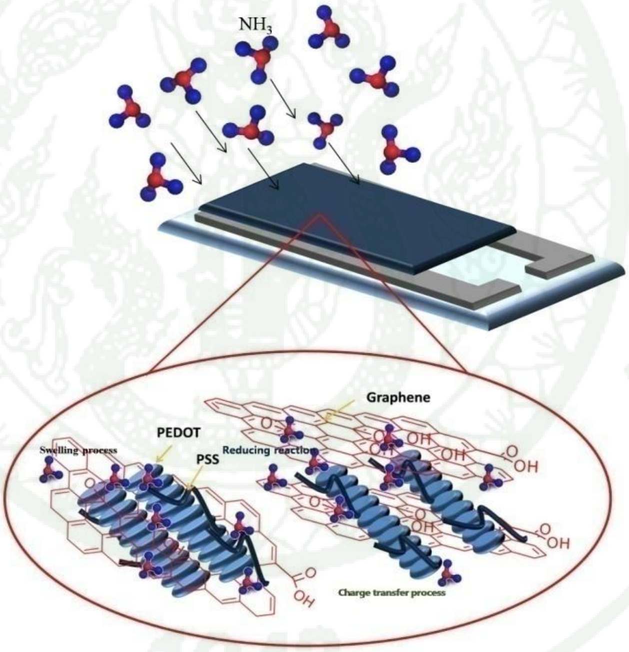

Figure 38 Schematic of sensing mechanism of graphene-PEDOT:PSS gas sensor

CONCLUSION AND RECOMMENDATION

Conclusion

From the experimental results and discussion of this study, the conclusion can be drawn as following;

(I) The development of flexible gas sensors has been successfully fabricated by using ink-jet printing technique

(II) From results of the effect of thickness of sensing films, the results indicate that the electrical resistance of the films decreases with increasing film thickness. The air humidity affects the based line resistance of gas sensor. The heating temperature of 90 ˚c for 20 min can correct the drift effect and recover the based line resistance to the original sensor fabrication.

(III) For the study of the response and selectivity of flexible printed PEDOT:PSS and graphene-PEDOT:PSS gas sensors, the results indicate that SEM, AFM, TEM, FTIR, UV-visible, and Raman characterizations confirm the presence of few-layer graphene in PEDOT:PSS polymer matrix and $\pi-\pi$ interactions between graphene and PEDOT:PSS. The incorporation of graphene in PEDOT:PSS leads to considerable enhancement of the gas response, dynamic property and selectivity to NH_3 due to the increase of the specific surface area, intrinsic sensing properties of graphene, and π electron interaction by graphene. The flexible PEDOT:PSS gas sensor exhibits high sensing performance for NH_3 with concentration from 25 -1000 ppm at room temperature. The gas response increases with increasing the bending angle.

(IV) From study of sensing mechanisms, the results indicate that reducing reaction with chemisorbed oxygen, direct charge transfers and swelling process are among possible sensing mechanisms of the flexile printed gas sensor. The swelling process and direct charge transfers seem to be the most probable main contribution.

Recommendation

From the experimental results, the proposed technique offers several distinct advantages over some other methods including high sensing performances, low temperature processing, high productivity, simplicity and low cost. Moreover, it will be useful for development of future wearable electronic technology.

LITERATURE CITED

Crowleya, K., A. Morrina, A. Hernandeza, E. O'Malleya, P. G. Whittenb,G. G.Wallace , M. R. Smytha, and A. J. Killarda. 2008. Fabrication of an ammonia gas sensor using inkjet-printed polyaniline nanoparticles. **Talanta** 7: 710-717.

Loffredoa, F., A. D. Girolamo Del Mauroa, G. Burrascaa, V. L. Ferraraa, L. Querciab, E. Masseraa, G. D. Franciaa, and D. D. Salab. 2009. Ink-jet printing technique in polymer/carbon black sensing device fabrication. **Sens. Actuators B** 143: 421-429.

Huang, L., Y. Huang, J. Liang, X. Wan, and Y. Chen. 2011. Graphene-Based Conducting Inks for Direct Inkjet Printing of Flexible Conductive Patterns and Their Applications in Electric Circuits and Chemical Sensors. **Nano Res.** 4(7): 675-684.

Wongchoosuk, C., P. Jangtawee, P. Lokavee, S. Udomrat, P. Sudkeaw, and T.Kerdcharoen. 2012. Novel flexible NH3 gas sensor prepared by ink-jet printing technique. **Adv. Mater. Res.** 506: 39.

Shena, W., 2012. Properties of SnO2 based gas-sensing thin films prepared by ink-jet printing. **Sens. Actuators B** 166-167: 110-116.

Xu, Y., Y. Wang, J. Liang, Y. Huang, Y. Ma, X. Wan, and Y. Chen. 2009. A hybrid material of graphene and poly (3,4-ethyldioxythiophene) with high conductivity, flexibility, and transparency. **Nano Res.** 2: 343-348.

Lu, L., O. Zhang, J. Xu, Y. Wen, X. Duan, H. Yu, L. Wu, and T. Nie. 2013. A facile one-step redox route for the synthesis of graphene/poly (3,4ethylenedioxythiophene) nanocomposite and their applications in biosensing. **Sens. Actuators B** 181: 567-574.

Mabrook, M.F., C. Pearson,and M.C. Petty. 2006. Inkjet-printed polymer films for the detection of organic vapors**. IEEE Sensor J.** 6: 1435.

Singh, M., H.M. Haverinen, P. Dhagat,and G.E. Jabbour. 2010. Inkjet printing-process and its applications. **Adv. Mater.** 22: 673-685.

Bai, H. and G. Shi. 2007. Gas Sensors Based on Conducting Polymers. **Sensors** 7: 267-307.

Nylabder, C., Armgrath, M. and Lundstrom, I. 1983. An ammonia detector based on a conducting polymer. **Proceedings of the International Meeting on Chemical Sensors, Fukuoka, Japan.** 203-207.

Shi, G.Q., Jin, S., Xue, G., and Li, C. 1995. A conducting polymer film stronger than aluminum. **Science** 267:994-996.

Groenendaal, L., F. Jonas, D. Freitag, H. Pielartzik, and J. R. Reynolds. 2000. Poly(3,4-ethylenedioxythiophene) and Its Derivatives: Past, Present, and Future. **Adv. Mater.** 12: 7.

Kim, J.Y., J. H. Jung, D. E. Lee, and J. Joo. 2002. Enhancement of electrical conductivity of poly(3,4-ethylenedioxythiophene)/poly(4-styrenesulfonate) by a change of solvents. **Synth. Met.** 126: 311–316.

Novoselov, K., A.Geim, S.Morozov, D. Jiang, Y. Zhang, S. Dubonos, I. Grigorieva, and A. Firsov. 2004.Electric field effect in atomically thin carbon films. **Science** 306: 666.

Hakimi, M. and P.Alimard. 2012. Graphene: Synthesis and applications in biotechnology - a review. **World Applied Programming** 2: 6.

Stankovich, S., D.A. Dikin, R.D. Piner, K.A. Kohlhaas, A. Kleinhammes, Y. Jia, y. Wu, S. B. T. Nguyen, and R. S. Ruoff. 2007. Synthesis of graphene-based nanosheets via chemical reduction of exfoliated graphite oxide. **Carbon** 45: 1558.

May, J.W. 1969. Platinum surface LEED rings. **Surf. Sci**. 17:267.

Shelton, J.C., H.R. Patil, and J.M. Blakely. 1974.Equilibrium segregation of carbon to a nickel (111) surface: a surface phase transition. **Surf. Sci**. 43: 493.

Eizenberg, M., and J.M. Blakely. 1979. Carbon monolayer phase condensation on Ni (111). **Surf. Sci.** 82: 228.

Somani, P.R., S.P. Somani, and M. Umeno. 2006. Planer nano-graphenes from camphor by CVD. **Chem. Phys. Lett**. 430: 56.

Wang, J.J., M.Y. Zhu, R.A. Outlaw, X. Zhao, D.M. Manos, and B.C. Holoway. 2004. Synthesis of carbon nanosheets by inductively coupled radiofrequency plasma enhanced chemical vapor deposition. **Carbon** 42: 2867.

Hummers, W.O.R. 1958. Preparation of graphite oxide. **J. Am. Chem. Soc.** 80: 1339.

Ni, Z., Y. Wang, T. Yu, and Z. Shen. 2008. Raman spectroscopy and imaging of graphene. **Nano Res.** 1: 273-291.

Geim, A. K., and K. S. Novoselov. 2007. The rise of graphene. **Nature Materials** 6: 183-191.

Chen, J. H., C. Jang, S. Xiao, M. Ishigami, and M. S. Fuhrer. 2008. Intrinsic and extrinsic performance limits of graphene devices on SiO_2. **Nature Nanotechnology** 3: 206-209.

Lee, C., X. Wei, J. W. Kysar, and J. Hone.2008. Measurement of the elastic properties and intrinsic strength of monolayer graphene. **Science** 321: 385-388.

Braga, S., V. R. Coluci, S. B. Legoas, R. Giro, D. S. Galvão, and R. H. Baughman. 2004. Structure and Dynamics of Carbon Nanoscrolls. **Nano Letters** 4 (5): 881.

Frank, I. W., D. M. Tanenbaum, A.M. Van Der Zande, and P. L. McEuen 2007. Mechanical properties of suspended graphene sheets. **J. Vac. Sci. Technol. B** 25(6): 2558-2561.

Kuzmenko, A. B., Van Heumen, E., Carbone, F., and Van Der Marel, D. 2008. Universal infrared conductance of graphite. **Physical Review Letters** 100 (11): 117401.

Zhang, Y., T.-T. Tang, C. Girit, Z. Hao, M. C. Martin, A. Zettl, M. F. Crommie., Y. Ron Shen, and F. Wang. 2009. Direct observation of a widely tunable bandgap in bilayer graphene. **Nature** 459 (7248): 820-823.

Junfeng, L., A. R. Wright, C. Zhang, and Z. Ma. 2008. Strong terahertz conductance of graphene nanoribbons under a magnetic field. **Appl Phys Lett** 93 (4): 041106-041110.

Kürüm, U., O. Ö. Ekiz, H. G. Yaglioglu, A. Elmali, M. Ürel, H. Güner, A. K. Mızrak, B. Ortac, and A. Dâna. 2011. Electrochemically tunable ultrafast optical response of graphene oxide. **Appl. Phys. Lett**. 98: 141103.

Lina, C.-Y., J.-G. Chena, C.-W. Hub, J.J. Tunneyc, and K.-C. Hoa. 2009. Using a PEDOT:PSS modified electrode for detecting nitric oxide gas. **Sens. Actuators B** 140: 402-406.

Bai, H., and G. Shi. 2007. Gas sensors based on conducting polymers, **Sensors** 7: 267-307.

Weber, E.-H. 1970. Room-temperature chemisorption mechanism of oxygen at CdS surfaces by photoconductivity investigations, **Physica status solidi**. 1: 665–678.

Gautam, M., and A.H. Jayatissa. 2012. Ammonia gas sensing behavior of graphene surface decorated with gold nanoparticles. **Solid-State Electron**. 78: 159–165.

Wu, Z., X. Chen, S. Zhu, Z. Zhou, Y. Yao, W. Quan, and B. Liu. 2013. Enhanced sensitivity of ammonia sensor using graphene/polyaniline nanocomposite. **Sens. Actuators B** 178: 485- 493.

Kwon, O.S., E. Park, O.Y. Kweon, S.J. Park, and J. Jang. 2010. Novel flexible chemical gas sensor based on poly(3,4-ethylene dioxythiophene) nanotube membrane. **Talanta** 82 : 1338-1343.

Jian, J., X. Guo, L. Lin, Q. Cai, J. Cheng, and J. Li. 2013. Gas-sensing characteristics of dielectrophoretically assembled composite film of oxygen plasma-treated SWCNTs and PEDOT/PSS polymer. **Sens. Actuators B** 178: 279-288.

Crispin, X., S. Marciniak, W. Osikowicz, G. Zotti, A.W. Denier Vander Gon, F. Louwet, M. Fahlman, L. Groenendaal, F. Deschryver, and W.R. Salaneck. 2003. Conductivity, morphology, interfacial chemistry, and stability of poly(3,4-ethylene dioxythiophene)-poly(styrenesulfonate): a photoelectron spectroscopy study. **J. Polym. Sci. B: Polym. Phys.** 41: 2561-2583.

Lee, Y.-L., C.-Y. Sheu, and R.-H. Hsiao. 2004. Gas sensing characteristics of copper phthalocyanine films: effects of film thickness and sensing temperature. **Sens. Actuators B** 99: 281.

Yue, G., J. Wu, Y. Xiao, J. Lin, M. Huang, Z. Lan, and L. Fan. 2013. Functionalized graphene/poly(3,4ethylenedioxythiophene)-polystyrenesulfonate as counter electrode catalyst for dye-sensitized solar cells. **Energy** 54: 315-321.

Kim, Y.H., C. Sachse, M.L. Machala, C. May, L.M.-Meskamp, and K. Leo. 2011. Highly conductive PEDOT:PSS electrode with optimized solvent and thermal post-treatment for ITO-free organic solar cells. **Adv. Funct. Mater.** 21: 076-1081.

Nemade, K.R. Waghuley, S.A. 2013. LPG sensing application of graphene/Bi_2O_3 quantum dots composites. **Solid State Sci.** 22:27-32.

Kim, G.H. Hwang, D.H. Woo, S.I. 2012. Thermoelectric properties of nanocomposite thin films prepared with poly(3,4-ethylenedioxythiophene) poly(styrenesulfonate) and graphene. **Phys. Chem. Chem. Phys.** 14:3530–3536.

Alexandre, M. Dubois, P. 2000. Polymer-layered silicate nanocomposites: preparation, properties and uses of a new class of materials. **Materials Science and Engineering** 28:1-63.

Xiong, S., L. Zhang, and X. Lu. 2013. Conductivities enhancement of poly(3,4-ethylenedioxythiophene)/poly(styrenesulfonate) transparent electrodes with diol additives. **Polym. Bull.** 70: 237-247.

Farah, A.A., S.A. Rutledge, A. Schaarschmidt, R. Lai, and J.P. Freedman. 2012. Conductivity enhancement of poly(3,4-ethylenedioxythiophene)-poly(styrenesulfonate) films post-spincasting. **J. Appl. Phys.** 112: 113709.

Barba, M. S. and A.M. Kelley. 2010. Surface-enhanced raman study of the Interaction of PEDOT:PSS with plasmonically active nanoparticles. **J. Phys. Chem. C** 114: 6822-6830.

Kim, G.H., D.H. Hwang, and S.I. Woo. 2012. Thermoelectric properties of nanocomposite thin films prepared with poly(3,4-ethylenedioxythiophene) poly(styrenesulfonate) and graphene. **Phys. Chem. Chem. Phys**. 14: 3530-3536.

Ferrari, A.C., J.C. Meyer, V. Scardaci, C. Casiraghi, M. Lazzeri, F. Mauri, S. Piscanec, D. Jiang, K.S. Novoselov, S. Roth, and A.K. Geim. 2006. Raman spectrum of graphene and graphene layers. **PRL.** 97: 187401.

Ghadim, E. E., F. Manouchehri, G. Soleimani, H. Hosseini, S. Kimiagar, and S. Nafisi. 2013. Adsorption properties of tetracycline onto graphene oxide: equilibrium, kinetic and thermodynamic studies. **PLOS ONE** 8: 79254.

Weng, B., F. Xu, and K. Lozano. 2014. Mass production of carbon nanotube-reinforced polyacrylonitrile fine composite Fibers. **J. APPL. POLYM. SCI**. 131: 40302.

Chu, C.-Y., J.-T. Tsaia, and C.-L. Sun. 2012. Synthesis of PEDOT-modified graphene composite materials as flexible electrodes for energy storage and conversion applications. **Int. J. Hydrogen Energy**. 37: 13880-1386.

Acik, M., G. Lee, C. Mattevi, M. Chhowalla, K. Cho, and Y. J. Chabal. 2010. Unusual infrared-absorption mechanism in thermally reduced graphene oxide. **Nature Materials**. 9: 840- 845.

Stankovich, S., R. D. Piner, S. T. Nguyen, and R. S. Ruoff. 2006. Synthesis and exfoliation of isocyanate-treated graphene oxide nanoplatelets. **Carbon** 44: 3342–3347.

Mandal, A., and A. K. Nandi. 2012. Noncovalent functionalization of multiwalled carbon nanotube by a polythiophene-based compatibilizer: reinforcement and conductivity improvement in Poly(vinylidene fluoride) films. **J. Phys. Chem. C** 116: 9360−9371.

Si, W., W. Lei, Y. Zhanga, M. Xiaa, F. Wanga, and Q. Haob. 2012. Electrodeposition of graphene oxide doped poly(3,4-ethylenedioxythiophene) film and its electrochemical sensing of catechol and hydroquinone. **Electrochimica Acta** 85: 295-301.

Sriprajuabwong, C., C. Karuwan, D. Phokharatkul, A. Wisitsoraat, and A. Tuantranont. 2012. Inkjet-printed graphene-PEDOT:PSS modified screen printed carbon electrode for biochemical sensing. **J. Mater. Chem** 22: 5478-5485.

Zhang, S., J. Hou, R. Zhang, J. Xu, G. Nie, and S. Pu. 2006. Electrochemical polymerization of 3,4-ethylenedioxythiophene in aqueous solution containing N-dodecyl 1-β-D-maltoside. **Eur. Polym. J.** 42: 149-160.

Karuwan, C., C. Sriprachuabwong, A. Wisitsoraat, D. Phokharatkul, P. Sritongkham, and A. Tuantranont. 2012. Inkjet-printed graphene-poly(3,4ethylenedioxythiophene) :poly(styrene-sulfonate) modified on screen printed carbon electrode for electrochemical sensing of salbutamol. **Sens. Actuators B** 161: 549-555.

Kvarnstrom, C., H. Neugebauer, A. Ivaska, and N.S. Sariciftci. 2000. Vibrational signatures of electrochemical p and n-doping of poly(3,4-ethylenedioxythiophene) films: an in situ attenuated total reflection Fourier transform infrared (ATR-FTIR) study. **J. Mol. Struct.** 521: 271-277.

Ricardo, K. B., A. Sendecki, and H. Liu. 2014. Surfactant-free exfoliation of graphite in aqueous solutions. **Chem. Commun.** 50: 2751.

Sun, K., Y. Xia, and J. Ouyang. 2012. Improvement in the photovoltaic efficiency of polymer solar cells by treating the poly (3,4ethylenedioxythiophene) :poly(styrenesulfonate) buffer layer with co-solvents of hydrophilic organic solvents and hydrophobic 1,2-dichlorobenzene. **Solar Energy Materials and Solar Cells**. 97: 89–96.

Trang, L. K. H., T. T. Tung, T. Y. Kim, W. S. Yang, H. Kimb, and K. S. Suh. 2012. Preparation and characterization of graphene composites with conducting polymers. **Polym Int.** 61:93–98.

KvarnstroÈm, C., H. Neugebauer, S. Blomquist, H.J. Ahonen, J. Kankare, and A. Ivaska. 1999. In situ spectroelectrochemical characterization of poly(3,4-ethylenedioxythiophene). **Electrochim. Acta** 44: 2739-2750.

Suchea, M. Katsarakis, N. Christoulakis, S. Nikolopoulou, S. Kiriakidis, G. 2006. Low temperature indium oxide gas sensors. **Sens. Actuators B** 118: 135–141.

Romero, H. E., Prasoon, J., Awnish, K. G., Humberto R G., Milton W.C., Srinivas A. T., Peter C. E., 2009. Adsorption of ammonia on graphene, **Nanotechnology** 20: 245501.

Huang, X., Hu, N., Gao, N., Yu, Y., Wang, Y., Yang, Z., Eric Siu-Wai Kong, Weia, H., Zhang, Y., 2012. Reduced graphene oxide–polyaniline hybrid: Preparation, characterization and its applications for ammonia gas sensing**. J. Mater. Chem.** 22: 22488.

CURRICULUM VITAE

NAME : Yotsarayuth Seekaew, Mr.

DATE OF BIRTH : June 29, 1988

PLACE OF BIRTH : Khon Kaen, Thailand

EDUCATION :

YEAR	**INSTITUTE**	**DEGREE/DIPLOMA**
2010	Kasetsart Univ.	B.Sc. (Physics)

SCHOLARSHIP/AWARDS :

- M.Sc. Scholarship for International Publication from the Graduate School, Kasetsart University (2012)
- Teaching Assistantship from Department of Physics, Kasetsart University (2013-2014)

JOURNAL PUBLICATIONS:

1. Y. Seekaew, S. Lokavee, D. Phokharatkul, A. Wisitsoraat, T. Kerdcharoen, C. Wongchoosuk, "Low-Cost and Flexible Printed Graphene-PEDOT:PSS Gas Sensor for Ammonia Detection", Organic Electronics 2014 (Accepted 26 August 2014).

INTERNATIONAL CONFERENCE PROCEEDINGS:

1. Y. Seekaew, W. Klanritt, S. Promchaem, and C. Wongchoosuk, Invention of Stereo Electronic Nose for Mobile Robot, the 10th Asian Conference on Chemical Sensors: Chemical Sensors for the Sustainable Society (ACCS 2013), November 11-14, 2013, The Empress Hotel, Chiang Mai, Thailand.

NATIONAL CONFERENCE PROCEEDINGS:

1. Y. Seekaew, S. Lokavee, D. Phokharatkul, T. Kerdcharoen, C. Wongchoosuk, "Fabrication of Flexible Graphene-PEDOT/PSS Gas Sensor by Ink-Jet Printing Technique", Proceeding of Siam Physics Congress 2013 (SPC2013), 21-23 March 2013, Chaing Mai, Thailand.

2. Y. Seekaew, S. Lokavee, S. Chomkokard, T. Kerdcharoen, C. Wongchoosuk, "Effect of Thickness on Ethanol Gas Sensor Prepared by Ink-jet Printing Techique", Proceeding of the 38th Congress on Science and Technology of Thailand (STT-38), October 17-19, 2012, The Empress Convention Centre, *Chiang Mai, Thailand.